THE JOURNAL OF BIOLOGICAL CHEMISTRY VOL. 288, NO. 5, pp. 3070–3084, February 1, 2013

Dysregulation of Mitochondrial Calcium Signaling and Superoxide Flashes Cause Mitochondrial Genomic DNA Damage in Huntington Disease*

Received for publication, August 3, 2012, and in revised form, November 26, 2012 Published, JBC Papers in Press, December 17, 2012, DOI 10.1074/jbc.M112.407726

Jiu-Qiang Wang[‡], Qian Chen[‡], Xianhua Wang[§], Qiao-Chu Wang[‡], Yun Wang[‡], He-Ping Cheng[§], Caixia Guo[¶], Qinmiao Sun[‡], Quan Chen[‡], and Tie-Shan Tang[‡1]

From the [‡]State Key Laboratory of Biomembrane and Membrane Biotechnology, Institute of Zoology, Chinese Academy of Sciences, Beijing 100101, the [§]State Key Laboratory of Biomembrane and Membrane Biotechnology, Institute of Molecular Medicine, Peking University, Beijing 100871, and the [¶]Laboratory of Disease Genomics and Individual Medicine, Beijing Institute of Genomics, Chinese Academy of Sciences, Beijing 100029, China

Background: Oxidative damage has been implicated in the pathology of Huntington disease (HD).
Results: Strikingly higher mitochondrial Ca^{2+} loading and superoxide generation cause significantly higher levels of mitochondrial DNA damage in HD cells.
Conclusion: Excessive mitochondrial Ca^{2+} loading-dependent oxidant generation is a causative factor for HD.
Significance: Our data reveal new links between dysregulated mitochondrial Ca^{2+} signaling and elevated oxidative DNA damage in HD.

Huntington disease (HD) is an inherited, fatal neurodegenerative disorder characterized by the progressive loss of striatal medium spiny neurons. Indications of oxidative stress are apparent in brain tissues from both HD patients and HD mouse models; however, the origin of this oxidant stress remains a mystery. Here, we used a yeast artificial chromosome transgenic mouse model of HD (YAC128) to investigate the potential connections between dysregulation of cytosolic Ca^{2+} signaling and mitochondrial oxidative damage in HD cells. We found that YAC128 mouse embryonic fibroblasts exhibit a strikingly higher level of mitochondrial matrix Ca^{2+} loading and elevated superoxide generation compared with WT cells, indicating that both mitochondrial Ca^{2+} signaling and superoxide generation are dysregulated in HD cells. The excessive mitochondrial oxidant stress is critically dependent on mitochondrial Ca^{2+} loading in HD cells, because blocking mitochondrial Ca^{2+} uptake abolished elevated superoxide generation. Similar results were obtained using neurons from HD model mice and fibroblast cells from HD patients. More importantly, mitochondrial Ca^{2+} loading in HD cells caused a 2-fold higher level of mitochondrial genomic DNA (mtDNA) damage due to the excessive oxidant generation. This study provides strong evidence to support a new causal link between dysregulated mitochondrial Ca^{2+} signaling, elevated mitochondrial oxidant stress, and mtDNA damage in HD. Our results also indicate that reducing mitochondrial Ca^{2+} uptake could be a therapeutic strategy for HD.

Huntington disease (HD)[2] is an inherited, progressive neurodegenerative disorder characterized by chorea, gradual but inexorable cognitive decline, and psychiatric disturbances (1, 2). At the genetic level, the disease is caused by an abnormal expansion of the CAG repeat located in exon 1 of huntingtin (*HTT*), the gene encoding the huntingtin protein (3). A number of lines of evidence indicate that polyQ expansion in HTT (HTT^{exp}) leads to a "toxic gain of function" (4–15). Recent results suggest that HTT^{exp} toxicity may also involve disturbed glutamate-induced Ca^{2+} signaling in MSNs (9, 16). It has been reported that HTT^{exp} facilitates activity of NMDA receptors (15, 17–21) and type 1 inositol 1,4,5-trisphosphate receptors ($InsP_3R1$) (22, 23), leading to the enhanced intracellular Ca^{2+} signaling in HD neurons.

Oxidative damage may also contribute to neuronal loss in HD (24). Oxidative damage is clearly apparent in both HD patients and HD mouse models (25–29). Interestingly, oxidative damage in mitochondrial genomic DNA (mtDNA) preferentially occurs in the parietal region of the human HD brain, but not frontal cortex or cerebellum (26), and striatal MSN particularly accumulates more mtDNA mutations than any other brain cells (27), indicating the brain regional specificity of oxidative damage in HD. Deficiency of respiratory chain complexes has been suggested in enhanced reactive oxygen species generation in the HD yeast model (30), and complex II and III defects have been detected in HD brain (31–33), suggesting that defects of respiratory chain complexes may cause mitochondrial dysfunction and ROS overproduction. However, no significant deficiency of respiratory chain complexes has been dem-

* This work was supported National Basic Research Program of China Grants 2011CB965003, 2012CB944702, 2011CB809102, NSFC30970931, and NSFC31130067 and Knowledge Innovation Program of Chinese Academy of Sciences Grant KSCX2-YW-R-148, and by the One-Hundred-Talent Program (to C. G. and Q. S.).
[1] To whom correspondence should be addressed: State Key Laboratory of Biomembrane and Membrane Biotechnology, 1 Beichen West Rd., Chaoyang District, Beijing, 100101, China. Tel.: 86-10-64807296; Fax: 86-10-64807313; E-mail: tangtsh@ioz.ac.cn.

[2] The abbreviations used are: HD, Huntington disease; MEF, mouse embryonic fibroblast; MSN, medium spiny neuron; DHPG, (*RS*)-3,5-dihydroxyphenylglycine; BK, bradykinin; $InsP_3R$, inositol 1,4,5-trisphosphate receptor; MCU, mitochondrial Ca^{2+} uniporter; cpYFP, circular permuted yellow fluorescent protein; qPCR, quantitative PCR; 2-APB, 2-aminoethoxydiphenyl borate; ER, endoplasmic reticulum; ROS, reactive oxygen species; mPTP, mitochondrial permeability transition pore.

onstrated in presymptomatic patients or in HD model mice expressing full-length HTT^{exp}, suggesting that respiratory chain defects are a secondary feature in HD pathogenesis (34, 35). Therefore, the mechanism by which HTT^{exp} causes elevated oxidant stress in HD neurons remains elusive, and why striatal MSN are preferentially under oxidant stress is not known.

Enhanced cytosolic Ca^{2+} signaling in striatal MSN has been linked to neuropathology in HD (18, 22, 23). Mitochondrion is not only a very efficient Ca^{2+} buffer system but also constitutes the major ROS generator in eukaryotic cells, including neurons. We aim to look at the potential connection between mitochondrial Ca^{2+} loading and ROS generation in HD cells/neurons. However, whether Ca^{2+} loading into mitochondria matrix stimulates or decreases ROS generation is a topic of great debate in the field. From a thermodynamic point of view, it has been noted that Ca^{2+} loading into mitochondria, which consumes mitochondrial membrane potential ($\Delta\Psi_m$), should result in a partial uncoupling and thus would reduce electron flow from complex II and decrease ROS generation (36). However, a fundamentally different model has been proposed that mitochondrial matrix Ca^{2+} loading-induced uncoupling leads to increased ROS generation by virtue of increased in electron flux (to restore and to maintain $\Delta\Psi_m$), and thus increased in the probability of electron slippage and superoxide formation (37, 38). Both models were supported experimentally; however, the lack of specific ROS probes targeted to the mitochondria of living cells may be the main reason for this discrepancy. Nevertheless, Ca^{2+} signaling system may regulate components of ROS homeostasis and thus influence the redox balance in cells (38, 39), raising the possibility that excessive Ca^{2+} loading into mitochondria creates mitochondrial oxidant stress.

To dissect the molecular events between disrupted cytosolic Ca^{2+} signaling and mitochondrial oxidant stress, it is essential to visualize and quantify mitochondrial matrix ROS generation *in situ* and in real time. Recently, Wang *et al.* (40, 41) developed a highly sensitive mitochondrially targeted superoxide indicator, circular permuted yellow fluorescent protein (cpYFP), which can sense bursts of superoxide generation (termed superoxide flashes) in single mitochondrion in live cells. Moreover, mitochondrial matrix Ca^{2+} dynamics were also visualized by a mitochondria matrix-targeted Ca^{2+} indicator, cameleon (42, 43). We found that both mitochondrial Ca^{2+} signaling and superoxide generation are dysregulated in embryonic fibroblasts and striatal neurons from a yeast artificial chromosome transgenic mouse model of HD. We then provided direct evidence to support a new causal link between dysregulated mitochondrial Ca^{2+} signaling, elevated mitochondrial oxidant stress, and mtDNA damage accumulation in HD. Steady buildup of oxidative damage to mitochondrial DNA and proteins could eventually result in mitochondrial dysfunction and the defects of respiratory chain complexes found in postmortem studies of symptomatic HD patients (31–33). Because dysregulation of cytosolic Ca^{2+} signaling occurs preferentially in striatal neurons of HD (18, 21, 22), excessive mitochondrial Ca^{2+} loading and elevated mitochondrial oxidant stress are expected to affect striatal region selectively. Given that dysregulation of intracellular Ca^{2+} signaling has been linked to many pathological conditions (16, 44–48), our data also suggest that reducing mitochondrial Ca^{2+} uptake could form part of a therapeutic approach to slow the progression of several neurodegenerative diseases, including HD.

EXPERIMENTAL PROCEDURES

MEF and Primary MSN Cultures—YAC128 HD transgenic mice were obtained from The Jackson Laboratory (Bar Harbor, ME). Generation and breeding of YAC128 HD transgenic mice (FVBN/NJ background strain) have been described previously (49). Heterozygous male YAC128 mice were crossed with wild-type (WT) female mice. MEFs were isolated from 12.5 to 13.5 postcoitum mouse embryos as described previously (50) and genotyped by PCR with primers specific for exons 44 and 45 of *HTT*. The MEF cells were cultured in Dulbecco's modified Eagle's medium supplemented with 10% fetal bovine serum and immortalized through continuous passaging. Several immortalized MEF clones for each genotype were frozen for Ca^{2+} imaging and superoxide flash imaging experiments. Primary MSN cultures were established as described previously (23, 51).

Mitochondrial Ca^{2+} Imaging Experiments—Mitochondrial cameleon expression plasmid (pCDNA3.0–2mt-cameleon) was kindly provided by Dr. Roger Tsien (University of California, San Diego, La Jolla) (42, 43). Immortalized WT and YAC128 MEFs were plated on 3.5-cm confocal dishes and grown to 60–80% confluency in DMEM supplemented with 10% FBS. MEFs were then transfected with pCDNA3.0–2mt-cameleon (42) using Lipofectamine 2000 (Invitrogen) according to the manufacturer's instructions. Cells were imaged 2 days later after transfection. For imaging experiments, cells were rinsed twice and then maintained in Hanks' balanced salt solution (HBSS, 142 mM NaCl, 5.6 mM KCl, 1 mM $MgCl_2$, 2 mM $CaCl_2$, 0.34 mM Na_2HPO_4, 0.44 mM KH_2PO_4, 4.2 mM $NaHCO_3$, 10 mM HEPES and 5.6 mM glucose, pH 7.4). The Ca^{2+} imaging experiments were performed using a Leica DMI6000B total internal reflection fluorescence microscope (Leica). Dual-emission ratio imaging of cameleon was accomplished using a BP420/10 excitation filter, a 440/520 dichroic mirror, and two emission filters (BP472/30 for cyan fluorescent protein and BP542/27 for YFP) that were alternated using a filter changer. Exposure times were typically 100 ms, and images were collected every 3 s. Base-line (50 s) measurements were acquired before the first pulse of bradykinin (BK). BK was dissolved in HBSS, and the working concentration was 2.5 μM. In some experiments, MEFs were preincubated with 2-aminoethoxydiphenyl borate (2-APB, 20 μM) or Ru360 (10 μM) for 30 min at room temperature before stimulating with BK.

MSN cultures that had been 13–14 days *in vitro* were transfected with pCDNA3.0–2mt-cameleon using Lipofectamine 2000 (Invitrogen) and then imaged 2 days later after transfection. The MSNs were rinsed twice and maintained in artificial cerebrospinal fluid (140 mM NaCl, 5 mM KCl, 1 mM $MgCl_2$, 2 mM $CaCl_2$, and 10 mM HEPES, pH 7.3) at room temperature throughout the experiments. The stock solution of (*RS*)-3,5-dihydroxyphenylglycine (DHPG) was dissolved in artificial cerebrospinal fluid, and the working concentration was 50 μM.

The free Ca^{2+} concentration in mitochondria was determined using the following equation (42): $R = R_{max}\,[Ca^{2+}]^n/(K_d'^n + [Ca^{2+}]^n)$, where $K_d' = 0.76$, $R_{max} = 105.3$, and $n = 0.74$.

Measurement of Superoxide Flashes in Mitochondria of Living Cells—We employed lentivirus-medicated gene transfer to express cpYFP in the mitochondrial matrix of WT and YAC128 MEFs. The superoxide flash measurement experiments (cpYFP imaging) were performed as described previously with modifications (40). Briefly, cells were rinsed twice, maintained in HBSS at room temperature, and then stimulated with BK. cpYFP was excited at 488 nm, and emission was collected at 500–550 nm. Amplitude of superoxide flashes ($\Delta F/F_0$) was expressed as $(F_{max} - F_{base})/(F_{base} - F_{background})$, where F_{max} represented the peak superoxide flash fluorescence recorded, and F_{base} represented the fluorescence recorded before the generation of superoxide flashes. In some experiments, MEFs were preincubated in 2-APB or Ru360 at room temperature for 30 min before stimulating with 5 μM BK. 13–14 days *in vitro* MSN cultures were transfected with plasmid encoding cpYFP using Lipofectamine 2000 and then imaged the next day. MSNs were rinsed twice and then maintained in artificial cerebrospinal fluid at room temperature throughout the whole superoxide flashes experiment. The base-line measurements were acquired over 8 min, and the treatment with BK or DHPG also lasted for 8 min.

Normal (GM02185C) and HD patient (GM09197) primary human fibroblasts were from Coriell Cell Repositories. Human fibroblasts were grown in minimal essential medium supplemented with 15% fetal bovine serum at 37 °C with 5% CO_2. Lentivirus-mediated gene transfer was employed to express cpYFP in the mitochondrial matrix of human fibroblasts, and cpYFP imaging was performed as described above.

Knockdown Experiments—The siRNA sequence was synthesized for IP3R1, IP3R2, and IP3R3. The sequences used were as follows: 5′-AGCAGACACGAUAGUGAAAdTdT-3′, 5′-GGGUCCUGGUUUUACAUUC-3′, and 5′-CCAUUCAAACAGCAUUCAU-3′ for IP3R1; 5′-CCGUAUCUCUUACAUGCUGUCCAUAdTdT-3′ for IP3R2; and 5′-CAAGCAGUCUGUAUUUGGUdTdT-3′ for IP3R3 (52, 53). Meanwhile, a nonspecific sequence was synthesized as negative control from the following sequence: 5′-UUCUCCGAACGUGUCACGUGAAAUUdTdT-3′ (53). Two days after siRNA transfection with RNAiMAX (Invitrogen), Western blot experiments were performed to confirm the efficiency of IP3R knockdown. MEFs were dissociated and cultured in confocal dishes 1 day after siRNA transfection and then were transfected with cameleon or cpYFP plasmids. Measurements of mitochondrial Ca^{2+} dynamics and superoxide flashes were carried out as described above.

Assessment of Mitochondrial DNA Damage—The extent of mitochondrial DNA damage was evaluated by using a previously described qPCR assay with modifications (54, 55). Briefly, WT and YAC128 MEFs, before and after repetitive BK stimulation (twice for 10 min, 2.5 μM of BK) without or with Ru360 and SS31 pretreatment, were rinsed twice with cold PBS and digested with 0.25% trypsin. Total DNA was extracted using a TIANamp genomic DNA kit (TIANGEN) according to the manufacturer's protocol. DNA concentration and the $A_{260}/_{280}$ ratio were measured using a SYNeRGY4 (Biotek) spectrophotometer. A 117-base pair (bp) mtDNA fragment was amplified by qPCR to quantify the relative mitochondrial genome DNA copy number in total DNA samples. We also amplified a 900-bp fragment of 18 S ribosome gene as a control to correct the 117-bp mtDNA copy number in qPCR. The qPCR cycling conditions were as follows: 75 °C for 2 min; 94 °C for 1 min; 94 °C for 15 s; 62 °C for 45 s, and 72 °C for 30 s (40 cycles), and 72 °C for 5 min. The data were analyzed using the $\Delta\Delta Ct$ method to reflect the relative mitochondrial genome copy number in 1.0 ng of total DNA. Standard PCRs were then carried out to further confirm the exact relative mitochondrial genome copy number using the 117-bp mitochondrial fragment primers and cycle numbers that were within the linear range of qPCR amplification. To assess mitochondrial DNA integrity, a 10.0-kilobase pair (kb) mitochondrial DNA fragment was then amplified by using same amount of mitochondrial DNA as templates. The PCR profile was as follows: 1 min at 94 °C, followed by 30 cycles of 40 s at 94 °C and 60 °C for 15 min. A final extension at 72 °C was performed for 10 min. The 10.0-kb PCR products were resolved on 1% agarose gels, whereas the 117-bp PCR products were resolved on 2% agarose gels. Ethidium bromide-stained products were imaged, and the density of the amplified bands was quantified using ImageJ software under Gel Analyzer Options. Amplification of the 10-kb mtDNA fragment was normalized to the amplification of the 117-bp mtDNA fragment, and the PCR signal from treated samples was compared with that from untreated control DNA that contained the same amount of mtDNA. DNA from control samples is defined as undamaged in this assay. Because the DNA polymerase amplifies only undamaged templates, the relative amplification ratio (A_D/A_O) is inversely proportional to the extent of damage. A_D = amount of amplification from damaged DNA sample (BK-stimulated); A_O = amount of amplification from undamaged DNA sample (no BK stimulation). The average lesion frequency per strand is calculated as $-\ln A_D/A_O$ as described previously (54, 55). The results are expressed as relative amplification ratio (A_D/A_O) and as lesion frequency per 10-kb per strand.

The primers used in these experiments were as follows: 5′-GCCAGCCTGACCCATAGCCATATTAT-3′ and 5′-GAGAGATTTTATGGGTGTATTGCGG-3′ for the 10-kb mitochondrial fragment; 5′-CCCAGCTACTACCATCATTCAAGT-3′ and 5′-GATGGTTTGGGAGATTGGTTGATG-3′ for the 117-bp mitochondrial fragment (54, 55); and 5′-CCGTGGCGGCGACGACCCAT-3′ and 5′-TGCCTGGTGGTGCCCTTCCG-3′ for the nuclear 18 S ribosome.

Drugs—BK and DHPG were purchased from Sigma. Ru360 and 2-APB were purchased from Merck. SS31 was a gift from Tao Ye (Laboratory of Chemical Genomics, Peking University Shenzhen Graduate School, China).

Statistics—Data were expressed as the means ± S.E., and statistical significance of differences between different groups was assessed using the independent samples *t* test or analysis of variance for repeated measures at the 95% level ($p < 0.05$).

Study Approval—All animal experiments were reviewed and approved by the Institute of Zoology Institutional Animal Care and Use Committee and were conducted according to the committee's guidelines.

RESULTS

Disrupted Mitochondrial Ca^{2+} Signaling in HD Cells—In our previous studies, we found that mutant huntingtin protein, HTT^{exp}, specifically binds to and facilitates InsP3R1 activity (22), suggesting that excessive cytoplasmic Ca^{2+} signaling may play an important role in HD pathogenesis (9, 23). Because of the close connection between mitochondria and the endoplasmic reticulum (ER) (56, 57), Ca^{2+} may rush into the mitochondria and cause excessive Ca^{2+} loading during Ca^{2+} mobilization. To monitor the mitochondrial Ca^{2+} concentration ($[Ca^{2+}]_m$) changes in HD cells, we took the advantage of a protein-based Ca^{2+} indicator, cameleon. Cameleon was targeted into mitochondria, and the free Ca^{2+} dynamics in the mitochondrial matrix were visualized using fluorescence resonance energy transfer (FRET) (42, 43). The free Ca^{2+} concentration in the mitochondria of WT and YAC128 MEF cells was continuously monitored by cameleon FRET imaging, and the data are presented as absolute Ca^{2+} concentration in micromoles (Fig. 1). On average, the basal mitochondrial Ca^{2+} concentration before BK treatment in YAC128 MEFs was significantly higher than that in WT MEFs (6.23 ± 0.19 μM *versus* 5.48 ± 0.23 μM, $p < 0.05$) (Fig. 1, *A–C*). Treatment with 2.5 μM BK caused significantly bigger mitochondrial Ca^{2+} transients in YAC128 MEFs than in WT cells (22.95 ± 2.1 μM *versus* 15.0 ± 1.2 μM, $p < 0.01$) (Fig. 1, *A–C*). To quantify the amount of Ca^{2+} that loaded into mitochondria during BK stimulation, we calculated the area (μM·s) below Ca^{2+} transient traces. Significantly, more Ca^{2+} was loaded into the mitochondria in YAC128 MEFs than in WT MEFs (2485 ± 218 μM·s *versus* 1155 ± 209 μM·s, $p < 0.01$) (Fig. 1*D*). Similar results were obtained using different WT and YAC128 MEF clones (data not show). In summary, mitochondria in YAC128 HD cells show significantly higher Ca^{2+} loading compared with WT cells, even in resting cells, suggesting that mitochondrial Ca^{2+} signaling in HD cells is dysregulated.

Involvement of $InsP_3Rs$ and Mitochondrial Ca^{2+} Uniporter (MCU) in the Disrupted Mitochondrial Ca^{2+} Signaling in HD Cells—$InsP_3R$ is involved in the abnormal Ca^{2+} signaling in HD (16, 22, 23); therefore, we next tested if Ca^{2+} release via $InsP_3R$ is important in the disrupted mitochondrial Ca^{2+} signaling. 2-APB, a membrane-permeable blocker of $InsP_3Rs$, can specifically block Ca^{2+} release from $InsP_3Rs$ (58, 59). We compared BK-induced mitochondrial Ca^{2+} signals in WT and YAC128 MEF cultures in the presence and absence of 2-APB. Preincubation with 20 μM 2-APB significantly decreased the BK-induced mitochondrial Ca^{2+} peak values in both WT and YAC128 MEFs ($p < 0.01$) (Fig. 2, *A*, *B* and *D*). Consistent with mitochondrial Ca^{2+} peak value results, 2-APB was able to significantly reduce the peak area of BK-induced mitochondrial Ca^{2+} transients in WT MEFs and YAC128 MEFs ($p < 0.05$, Fig. 2, *B* and *E*), indicating the important role of InsP3Rs in excessive mitochondrial Ca^{2+} loading in HD cells. Moreover, in resting cells, 2-APB significantly reduced the basal mitochondrial Ca^{2+} levels in YAC128 MEFs ($p < 0.05$) but not in WT MEFs ($p > 0.05$) (Fig. 2, *B* and *D*), suggesting that the higher basal mitochondrial Ca^{2+} levels seen in YAC128 MEFs also involved $InsP_3Rs$.

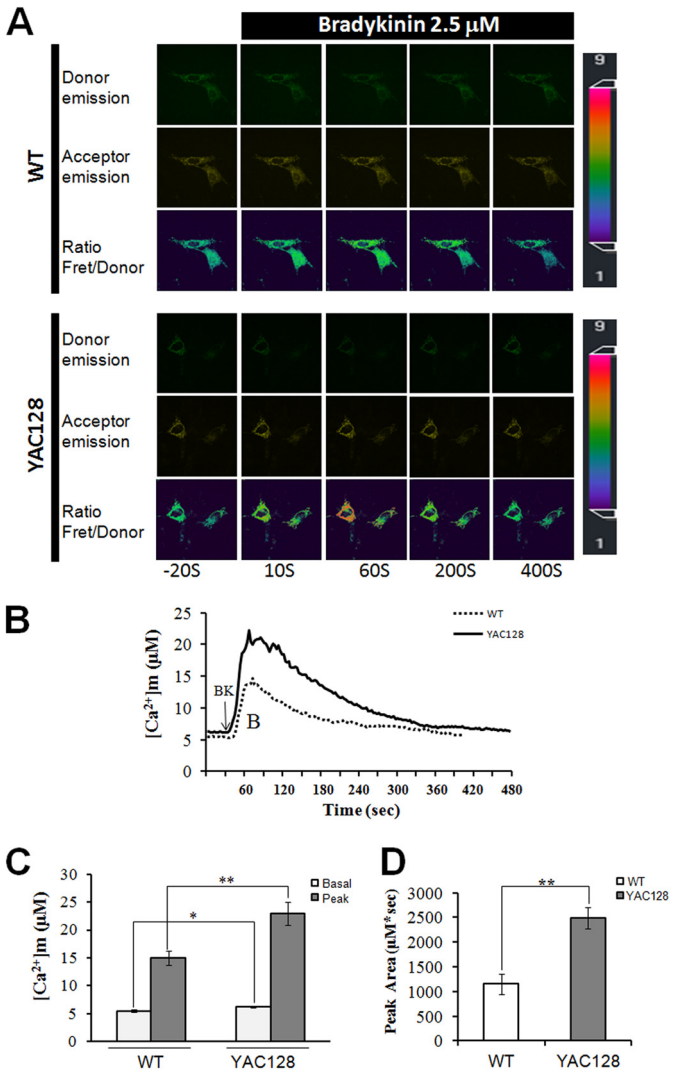

FIGURE 1. **Disrupted mitochondrial Ca^{2+} signaling in YAC128 MEFs.** *A*, representative mitochondrial cameleon images showing donor, acceptor, and ratio (*Fret/donor*) in WT and YAC128 MEFs. The pseudocolor calibration scale bar for Fret/donor ratios is shown on the *right*. Ratio recordings are shown for 2.5 μM bradykinin-induced mitochondrial Ca^{2+} transients in MEFs. *B*, absolute mitochondrial Ca^{2+} concentration ($[Ca^{2+}]_m$) changes in response to BK (2.5 μM) in WT ($n = 21$) and YAC128 ($n = 35$) MEFs. *C* and *D*, significantly larger $[Ca^{2+}]_m$ transients were found in YAC128 MEFs. Both basal and peak values (*C*) and peak areas (*D*) were significantly higher in YAC128 mitochondria than in WT mitochondria in response to BK (*, $p < 0.05$; **, $p < 0.01$). $[Ca^{2+}]_m$ traces in *B* are shown as an average of all cells in one experiment. Similar results were obtained in three independent experiments. Data are shown as the mean ± S.E.

There are three types of $InsP_3R$ ($InsP_3R1/2/3$), and which type of $InsP_3R$ is responsible for mitochondrial loading is not known. We performed $InsP_3R1/2/3$ siRNA knockdown experiments to address further the role of $InsP_3R$ in elevated mitochondrial calcium loading. The efficiency and selectivity of siRNA knockdown experiments were confirmed by Western blot with antibodies against $InsP_3R1/2/3$ (Fig. 2*F*). We found that knockdown of $InsP_3R1$ but not $InsP_3R2/3$ significantly reduced matrix Ca^{2+} loading in HD cells (Fig. 2, *G–L*), indicating that HTT^{exp}-induced elevated mitochondrial Ca^{2+} loading in HD cells was mainly mediated through type 1 $InsP_3R$. This is in agreement with our previous findings, which show that

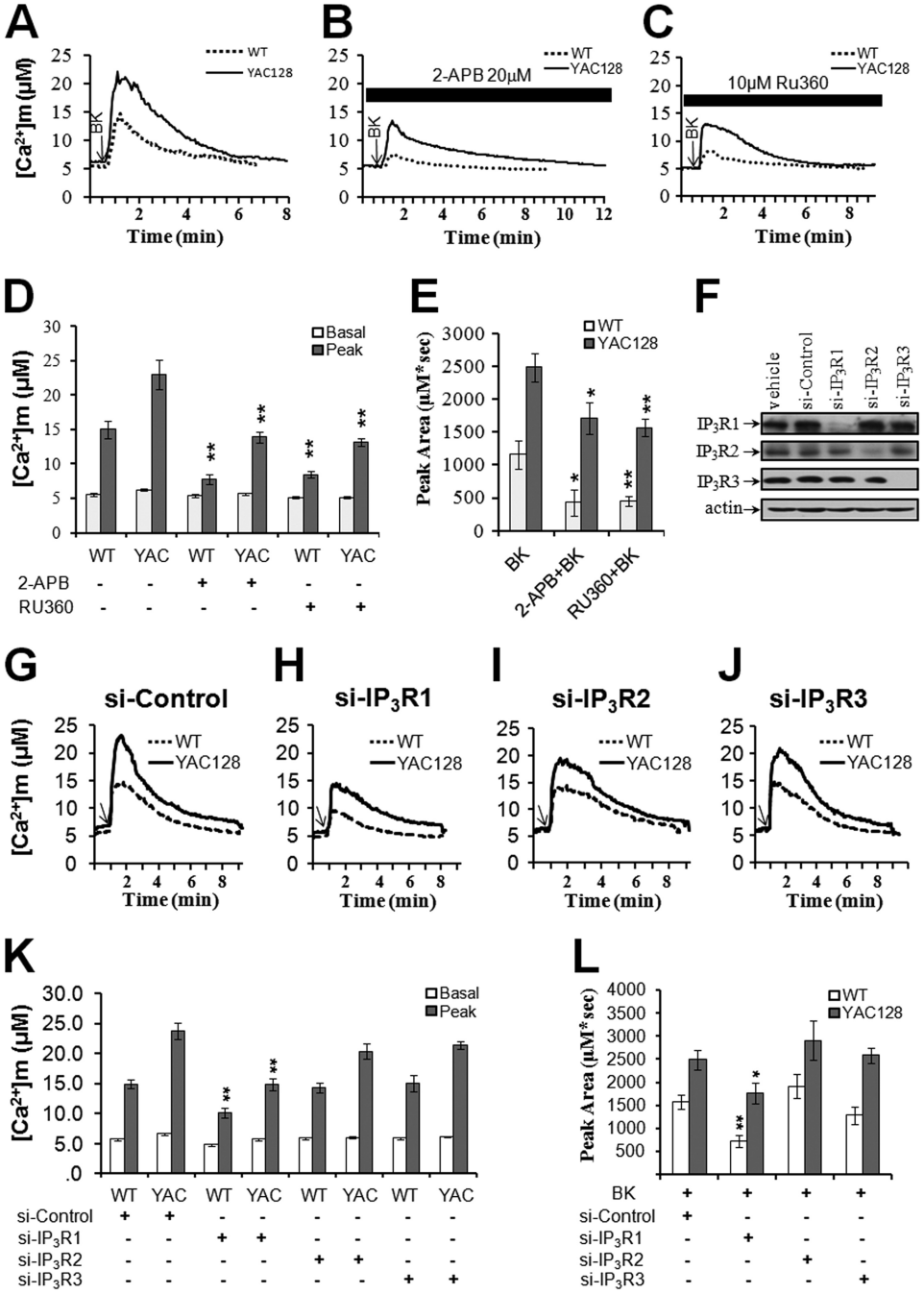

FIGURE 2. **Involvement of $InsP_3R1$ and MCU in the disrupted mitochondrial Ca^{2+} signaling in HD cells.** BK-induced $[Ca^{2+}]_m$ transients in WT and YAC128 MEFs were significantly reduced in the presence of the $InsP_3R$ blocker 2-APB (20 μM) (*B*) and MCU blocker Ru360 (10 μM) (*C*). Knockdown of $InsP_3R1$ (*H*) but not $InsP_3R2$ (*I*) and $InsP_3R3$ (*J*) was able to decrease BK-induced $[Ca^{2+}]_m$ transients. $[Ca^{2+}]_m$ traces in *A, B, C, G, H, I,* and *J* are shown as an average of all cells in one experiment. Similar results were obtained in three independent experiments. *D,* effect of 2-APB and Ru360 on the peak value of $[Ca^{2+}]_m$ in WT and YAC128 MEFs in response to BK. Pretreatment with 2-APB and Ru360 significantly decreased the peak value of $[Ca^{2+}]_m$ in both WT ($n = 21$ for 2-APB and $n = 29$ for Ru360) and YAC128 MEFs ($n = 34$ for 2-APB and $n = 22$ for Ru360) when compared with the control group (**, $p < 0.01$). *E,* effect of 2-APB and Ru360 on the peak area of $[Ca^{2+}]_m$ in WT and YAC128 MEFs in response to BK. Pretreatment with 2-APB and Ru360 significantly decreased the peak area of $[Ca^{2+}]_m$ in both WT and YAC128 MEFs when compared with the control group (*, $p < 0.05$; **, $p < 0.01$). Data are shown as the means ± S.E. *F,* efficiency and selectivity of siRNA knockdown were confirmed by Western blot with antibodies against $InsP_3R1$, $InsP_3R2$, and $InsP_3R3$, respectively. *K,* effect of knocking down $InsP_3R1/2/3$ on the peak value of $[Ca^{2+}]_m$ in WT and YAC128 MEFs in response to BK. Knockdown of $InsP_3R1$ significantly decreased the peak value of $[Ca^{2+}]_m$ in both WT ($n = 23$) and YAC128 MEFs ($n = 15$) when compared with the control group (**, $p < 0.01$). *L,* effect of knocking down $InsP_3R1/2/3$ on the peak area of $[Ca^{2+}]_m$ in WT and YAC128 MEFs in response to BK. Knockdown of $InsP_3R1$ significantly decreased the peak area of $[Ca^{2+}]_m$ in both WT and YAC128 MEFs when compared with the control group (*, $p < 0.05$; **, $p < 0.01$). Data are shown as the mean ± S.E.

mutant huntingtin protein facilitated the activity of $InsP_3R1$ (22, 23).

The MCU is located in the mitochondrial inner membrane and is considered the primary route of mitochondrial Ca^{2+} uptake (60). Consistent with the involvement of MCU in our experiments, preincubation of MEFs with the membrane-permeable MCU blocker, Ru360 (61), significantly decreased the amplitudes of BK-induced mitochondrial Ca^{2+} transients in

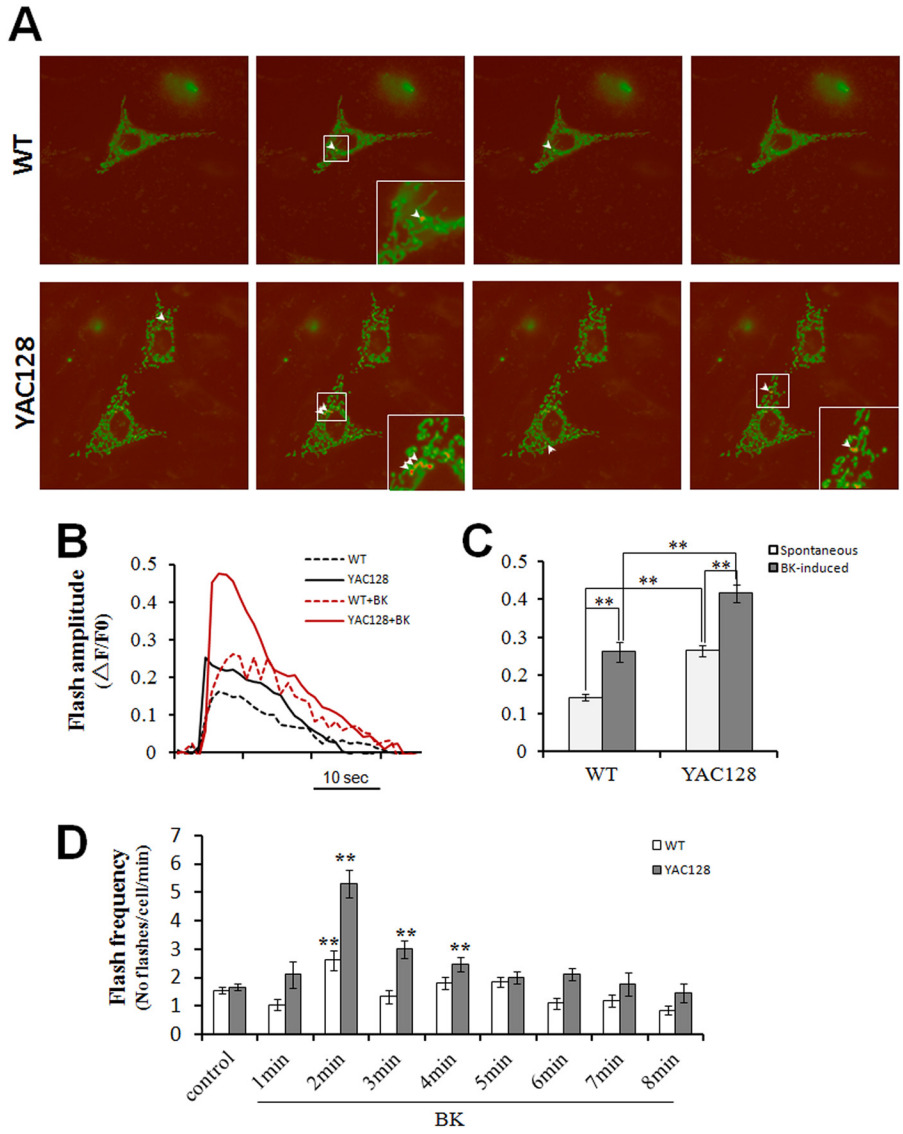

FIGURE 3. **BK promotes superoxide flash generation in YAC128 MEFs.** *A,* representative mt-cpYFP images showing superoxide flashes in mitochondria of WT and YAC128 MEFs. *Arrowheads* depict individual mitochondria with superoxide flashes. *Insets* are enlarged views showing mitochondria undergoing superoxide flashes. *B,* representative mitochondrial superoxide flash traces (mt-cpYFP fluorescence with excitation at 488 nm, $\Delta F/F_0$) in WT and YAC128 MEFs without or with 2.5 μM BK stimulation. *C* and *D,* statistical analysis of superoxide flashes in WT and YAC128 MEFs in response to 2.5 μM BK. *C,* in resting cells, the amplitude of spontaneous mitochondrial superoxide flashes in YAC128 ($n = 37$) MEFs was significantly higher than in WT MEFs ($n = 21$) (**, $p < 0.01$). In response to BK, both WT ($n = 21$) and YAC128 MEFs ($n = 17$) showed significantly higher amplitudes of superoxide flashes when compared with spontaneous flashes in resting MEFs (**, $p < 0.01$), and BK caused significantly higher superoxide flashes in YAC128 MEFs ($n = 17$) than in WT ($n = 21$) MEFs (**, $p < 0.01$). Flashes occurring 8 min before BK application and 8 min after BK application were averaged for superoxide flash amplitude analysis. *D,* in resting cells, spontaneous mitochondrial superoxide flashes occurred at a similar frequency in WT and YAC128 MEFs ($p > 0.05$). In response to BK, superoxide flashes in YAC128 MEFs occurred at a significantly higher frequency at 2–4 min after BK treatment when compared with resting cells (**, $p < 0.01$) and with WT MEFs (**, $p < 0.01$). Data are shown as the mean ± S.E.

both WT ($p < 0.05$) and YAC128 MEFs ($p < 0.01$) (Fig. 2, *C* and *D*), and it also reduced the amount of Ca^{2+} loaded into the mitochondria of both WT ($p < 0.01$) and YAC128 MEFs ($p < 0.01$) (Fig. 2, *C* and *E*). The resting mitochondrial Ca^{2+} levels were also significantly reduced in YAC128 MEFs in the presence of Ru360 ($p < 0.01$). Based on these results, we concluded that excessive mitochondrial Ca^{2+} loading in HD cells involved both InsP3Rs and MCU.

Excessive ROS Generation in YAC128 HD Cells—Compelling evidence suggests that oxidative damage contributes to neurodegeneration in HD. However, the origins of this oxidative stress remain unclear. ROS are primarily produced as by-products of mitochondrial respiration due to electrons leaking from the electron transfer chain, and accumulating data indicate that mitochondrial matrix Ca^{2+} is a positive effector of the tricarboxylic acid (TCA) cycle (62) and ROS generation (38, 39). The quantitative estimation of the mitochondrial matrix redox state *in situ* in live cells was not possible until the development of the highly sensitive superoxide indicator, cpYFP (40, 63). We therefore used cpYFP imaging to quantitatively compare the mitochondrial superoxide flashes between WT and YAC128 MEFs to determine the functional consequences of excessive mitochondrial Ca^{2+} loading in YAC128 HD cells (Fig. 3*A*). In resting cells, the amplitudes of spontaneous superoxide flashes was sig-

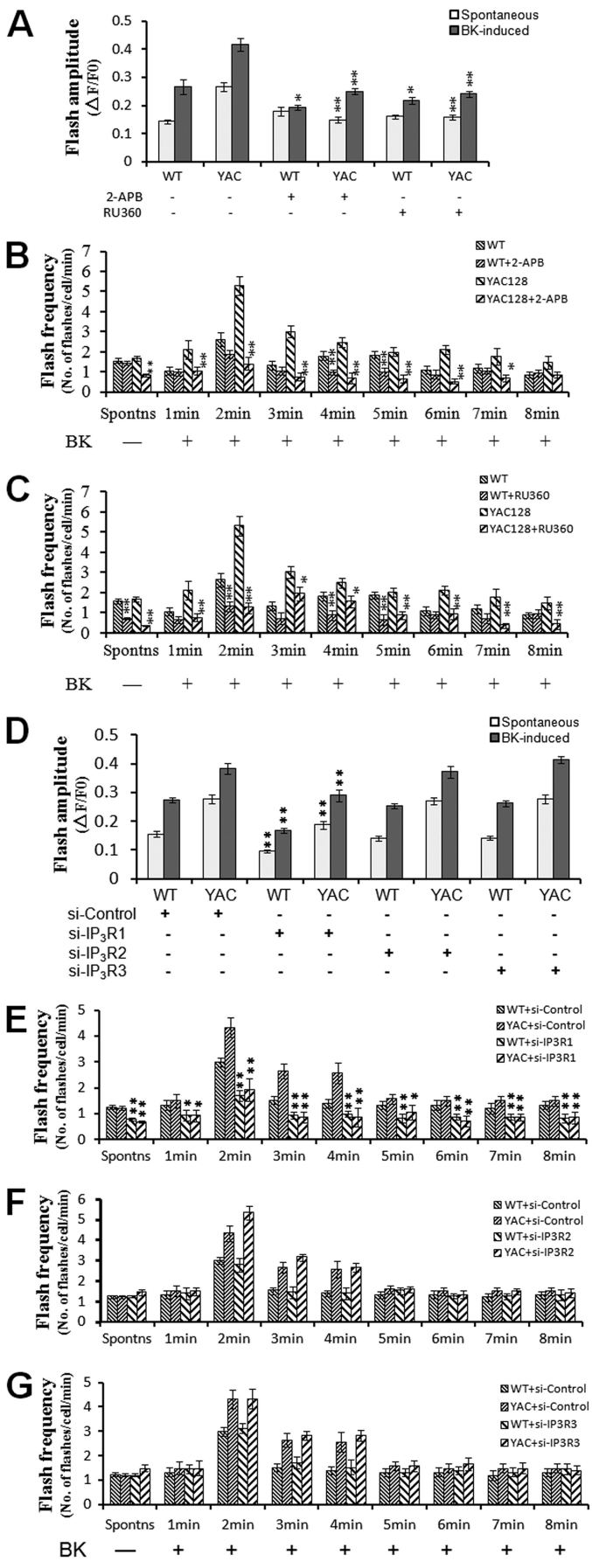

nificantly higher in YAC128 MEFs compared with WT MEFs (0.266 ± 0.015 *versus* 0.143 ± 0.008, $p < 0.01$) (Fig. 3, *A–C*). Stimulation with 2.5 μM BK significantly increased the amplitudes of superoxide flashes both in WT MEFs (0.263 ± 0.026 *versus* 0.143 ± 0.008 without BK, $p < 0.01$) and YAC128 MEFs (0.416 ± 0.022 *versus* 0.266 ± 0.015 without BK, $p < 0.01$) (Fig. 3, *B* and *C*). Furthermore, BK stimulated significantly higher amplitude flashes in YAC128 MEFs compared with WT MEFs (0.416 ± 0.022 *versus* 0.263 ± 0.026, $p < 0.01$) (Fig. 3, *B* and *C*). Because superoxide flashes occur randomly in space and time, we also quantified the number of flashes that occurred per min per cell to indicate the flash frequency. In resting cells, spontaneous superoxide flashes occurred at similar frequencies (flashes/min/cell) in WT and YAC128 MEFs (1.558 ± 0.118 and 1.676 ± 0.121, respectively, $p > 0.05$). However, in response to BK, WT MEFs exhibited a significantly higher superoxide flash frequency 2 min after BK application (2.619 ± 0.355 *versus* 1.558 ± 0.118, $p < 0.01$), whereas YAC128 MEFs exhibited significantly higher superoxide flash frequencies at 2 min (5.294 ± 0.476 *versus* 1.676 ± 0.121, $p < 0.01$), 3 min (3.00 ± 0.297 *versus* 1.676 ± 0.121, $p < 0.01$), and 4 min (2.471 ± 0.259 *versus* 1.676 ± 0.121, $p < 0.01$) after BK application compared with resting cells (Fig. 3*D*). More importantly, BK stimulated significantly higher flash frequencies in YAC128 MEFs compared with WT MEFs at 2–4 min ($p < 0.01$) after BK application (Fig. 3*D*). In summary, the amplitudes and frequencies of both spontaneous and BK-stimulated superoxide flashes are significantly higher in YAC128 MEFs compared with WT MEFs, indicating that mitochondria in HD cells produce elevated levels of oxidative stress.

FIGURE 4. **Role of mitochondrial Ca^{2+} overloading in the generation of superoxide flashes in WT and YAC128 MEFs.** *A,* effect of $InsP_3R$ blocker, 2-APB, and MCU blocker, Ru360, on mitochondrial superoxide flashes in WT and YAC128 MEFs. Pretreatment with 2-APB (20 μM) or Ru360 (10 μM) significantly decreased the amplitude of both spontaneous and BK-induced superoxide flashes in YAC128 MEFs ($n = 21$ for 2-APB and $n = 28$ for Ru360) compared with the control group (**, $p < 0.01$). For WT MEFs, however, 2-APB ($n = 17$) and Ru360 ($n = 20$) only caused significant reduction in the amplitude of BK-induced superoxide flashes (*, $p < 0.05$). *B,* effect of $InsP_3R$ blocker, 2-APB, on flash frequency in WT and YAC128 MEFs. Pretreatment of YAC128 MEFs with 2-APB resulted in a significantly lower spontaneous flash frequency and BK-induced flash frequency at 1–7 min after treatment when compared with the control group ($n = 21$, **, $p < 0.01$; *, $p < 0.05$). However, 2-APB only caused a significantly lower BK-induced flash frequency at 4 and 5 min after treatment ($n = 20$, *, $p < 0.01$) in WT MEFs. Data are shown as the mean ± S.E. *C,* effect of MCU blocker, Ru360, on flash frequency in WT and YAC128 MEFs. Pretreatment of YAC128 MEFs with Ru360 resulted in a significantly lower spontaneous flash frequency and BK-induced flash frequency at 1–8 min after treatment when compared with the control group ($n = 28$, **, $p < 0.01$; *, $p < 0.05$). Ru360 caused a significantly lower spontaneous flash frequency and BK-induced flash frequency only at 2, 4, and 5 min after treatment ($n = 20$, **, $p < 0.01$; *, $p < 0.05$) in WT MEFs. Data are shown as the mean ± S.E. *D,* effect of knockdown of $InsP_3R1/2/3$ on mitochondrial superoxide flashes in WT and YAC128 MEFs. Knockdown of $InsP_3R1$ significantly decreased the amplitude of both spontaneous and BK-induced superoxide flashes in YAC128 MEFs ($n = 31$) and in WT MEFs ($n = 35$) when compared with the siRNA control group (**, $p < 0.01$). In contrast, knockdown of $InsP_3R2/3$ failed to exhibit significant effect on flash amplitudes. *E–G,* effect of knockdown of $InsP_3R1/2/3$ on flash frequency in WT and YAC128 MEFs. Knockdown of $InsP_3R1$ in YAC128 and WT MEFs resulted in a significantly lower spontaneous flash frequency and BK-induced flash frequency at 1–8 min when compared with the siRNA control group ($n = 31$ for YAC128, $n = 35$ for WT, **, $p < 0.01$; *, $p < 0.05$). In contrast, knockdown of $InsP_3R2/3$ failed to exhibit significant effect on flash frequencies. Data are shown as the mean ± S.E.

Role of Mitochondrial Ca^{2+} Overloading in Excessive ROS Generation in YAC128 HD Cells—In the above mitochondrial Ca^{2+} and cpYFP imaging experiments, we demonstrated excessive mitochondrial Ca^{2+} loading (Figs. 1 and 2) and elevated ROS production (Fig. 3) in HD MEF cells. We next explored whether the elevated ROS production was dependent on mitochondrial Ca^{2+} influx. Pretreatment with 20 μM 2-APB or 10 μM Ru360 significantly attenuated the amplitudes of both spontaneous and BK-induced superoxide flashes in YAC128 MEFs compared with untreated control cells ($p < 0.01$) (Fig. 4 *A*). For WT MEFs, however, 2-APB and Ru360 caused significant reduction in the amplitudes of only the BK-induced superoxide flashes ($p < 0.01$) (Fig. 4*A*). As for flash frequency, both spontaneous and BK-induced superoxide flashes occurred at significantly lower frequencies in YAC128 MEFs in the presence of 2-APB or Ru360 ($p < 0.01$) (Fig. 4, *B* and *C*).

Specific knockdown of $InsP_3R1$ significantly reduced the amplitudes and flash frequencies of both spontaneous and BK-induced superoxide flashes in YAC128 MEFs compared with siRNA-control cells ($p < 0.01$) (Fig. 4, *D* and *E*), whereas knockdown of $InsP_3R2/3$ failed to elicit any significant effect on superoxide flash generation (Fig. 4, *F* and *G*), indicating the important role of type 1 $InsP_3R$ in augmenting oxidant stress in HD. All these results together demonstrate that elevated oxidative stress is critically dependent on excessive mitochondrial Ca^{2+} uptake in HD cells.

Disrupted Mitochondrial Ca^{2+} Signaling in YAC128 MSNs—To determine whether mitochondrial Ca^{2+} signaling is disturbed in HD neurons, we established MSN cultures from WT and YAC128 HD mice and compared the mitochondrial Ca^{2+} signaling dynamics between WT MSNs and YAC128 MSNs. DHPG, a selective group I metabotropic glutamate receptor agonist that can trigger $InsP_3$ production in MSNs, was used to stimulate intracellular Ca^{2+} mobilization in MSNs. Similar to the mitochondrial Ca^{2+} results in MEFs, in resting MSNs, the basal mitochondrial Ca^{2+} concentration before DHPG application in YAC128 MSNs was significantly higher than that in WT MSNs ($p < 0.05$) (Fig. 5, *A–C*). The difference in mitochondrial Ca^{2+} concentration between WT and YAC128 MSNs was even more pronounced during intracellular Ca^{2+} mobilization. Treatment with 50 μM DHPG caused much larger mitochondrial Ca^{2+} transients in YAC128 MSNs than in WT MSNs ($p < 0.01$) (Fig. 5, *A–C*). To quantify the amount of Ca^{2+} that was loaded into mitochondria during DHPG stimulation, we also calculated the peak area (μM·s) below each Ca^{2+} transient trace. Significantly more Ca^{2+} was loaded into mitochondria in YAC128 MSNs than in WT MSNs (547 ± 207 μM·s *versus* 135 ± 56.7 (μM·s, $p < 0.01$) (Fig. 5*D*). Therefore, mitochondria in YAC128 HD neurons show a significantly higher level of Ca^{2+} loading compared with WT neurons, further indicating that mitochondrial Ca^{2+} signaling is dysregulated in HD neurons.

Excessive ROS Generation in YAC128 HD Striatal Neurons—Excessive mitochondrial Ca^{2+} uptake caused elevated oxidative stress in YAC128 HD MEFs (Figs. 3 and 4). Next, we determined whether this was also true in YAC128 HD striatal medium spiny neurons. In resting MSNs, the amplitude of spontaneous superoxide flashes was significantly higher in

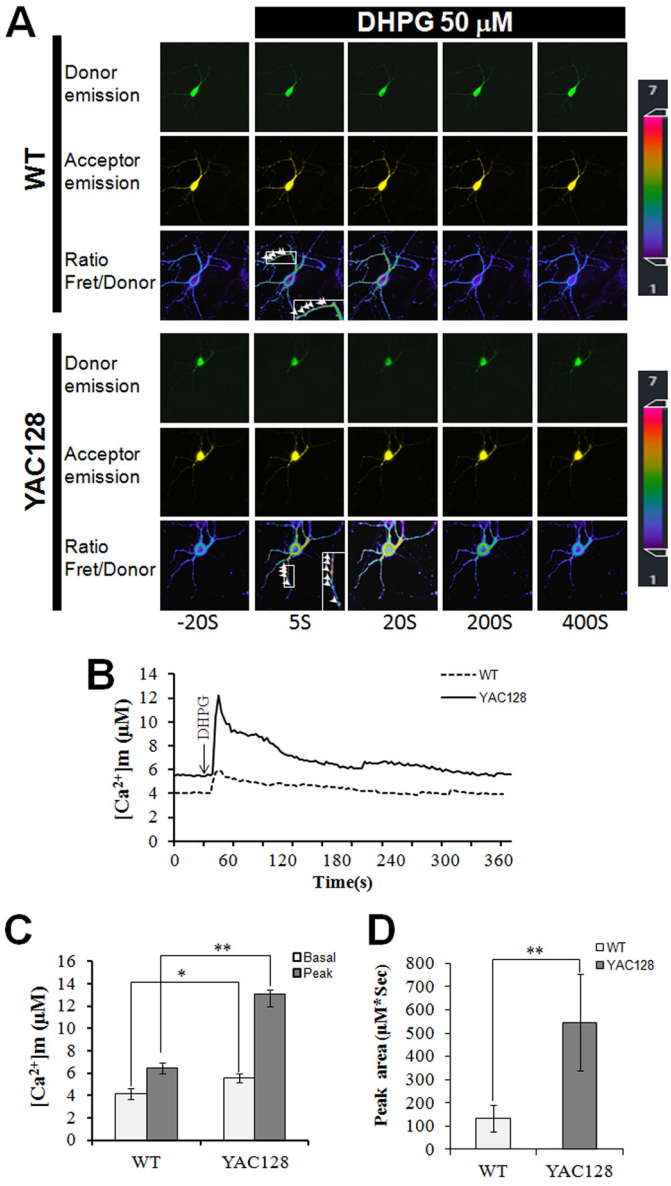

FIGURE 5. **Disrupted mitochondrial Ca^{2+} signaling in YAC128 MSNs.** *A,* representative mitochondrial cameleon images in MSNs showing donor, acceptor, and ratio (*Fret/donor*) images in WT and YAC128 MSNs. The pseudocolor calibration scale for Fret/donor ratios is shown on the *right*. Ratio recordings are shown for 50 μM DHPG-induced mitochondrial Ca^{2+} transients in MSNs. *Insets* are enlarged views for ratio images showing Ca^{2+} transients in MSN mitochondria. *B,* mitochondrial Ca^{2+} concentration ($[Ca^{2+}]_m$) traces in response to 50 μM DHPG in WT ($n = 12$) and YAC128 ($n = 6$) MSNs. *C* and *D,* significantly larger $[Ca^{2+}]_m$ transients were found in YAC128 MSNs. Both basal and peak values (*C*) and peak area (*D*) are significantly greater in YAC128 mitochondria than in WT mitochondria in response to DHPG (*, $p < 0.05$; **, $p < 0.01$). $[Ca^{2+}]_m$ traces in *B* are shown as an average of all cells in one experiment. Similar results were obtained in three independent experiments. Data are shown as the mean ± S.E.

YAC128 MSNs compared with that in WT MSNs ($p < 0.01$) (Fig. 6, *A–C*). Stimulation with 50 μM DHPG significantly increased the amplitudes of superoxide flashes both in WT MEFs ($p < 0.01$) and YAC128 MEFs ($p < 0.01$) compared with resting cells (Fig. 6, *B* and *C*). In addition, DHPG caused the amplitude of flashes to be significantly higher in YAC128 MSNs compared with WT MSNs ($p < 0.01$) (Fig. 6, *B* and *C*). Similarly to MEF cells, superoxide flashes in neurons also occur randomly. We monitored 5 min of neuronal flash events and cal-

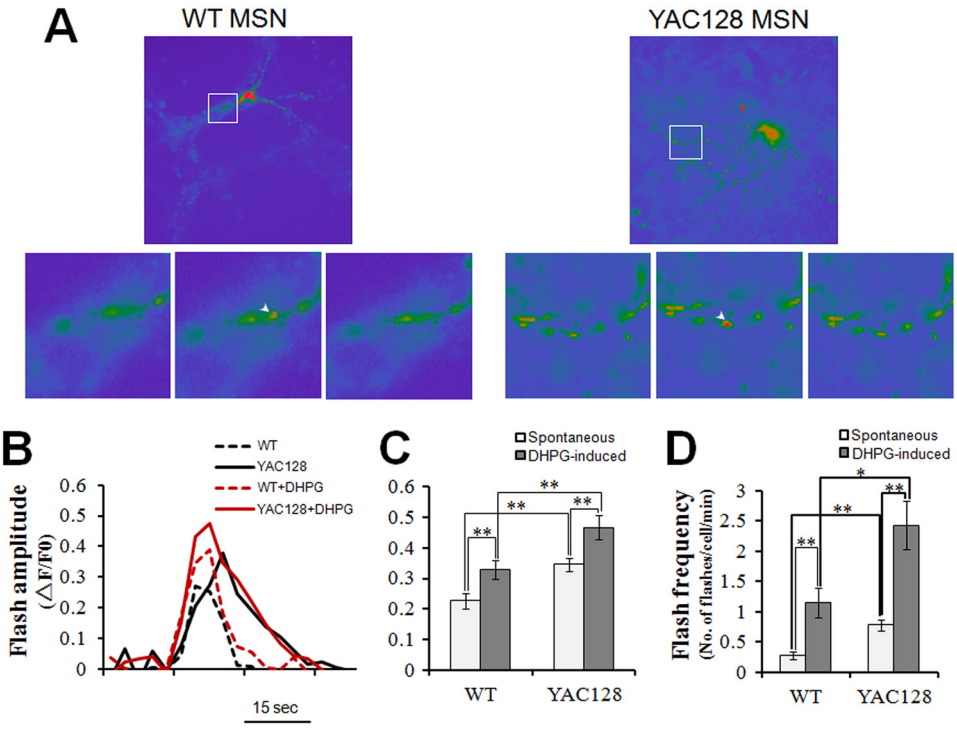

FIGURE 6. **DHPG promotes superoxide flash generation in YAC128 MSNs.** *A,* representative mt-cpYFP images showing mitochondrial superoxide flashes in WT and YAC128 MSNs. *Arrowheads* in *enlarged images* depict individual mitochondria with superoxide flashes. *B,* representative mitochondrial superoxide flash traces (mt-cpYFP fluorescence with excitation at 488 nm, $\Delta F/F_0$) in WT and YAC128 MSNs without or with 50 μM DHPG stimulation. *C* and *D,* statistical analysis of mitochondrial superoxide flashes in WT and YAC128 MSNs in response to 50 μM DHPG. *C,* in resting MSNs, the amplitude of mitochondrial superoxide flashes in YAC128 ($n = 12$) MSNs was significantly higher than that in WT MEFs ($n = 10$) (**, $p < 0.01$). In response to DHPG, both WT ($n = 11$) and YAC128 MSNs ($n = 7$) showed significantly higher superoxide flash amplitudes compared with spontaneous flashes in resting MSNs (**, $p < 0.01$), and DHPG caused significantly higher superoxide flash amplitudes in YAC128 MSNs ($n = 7$) compared with those in WT ($n = 11$) MSNs (**, $p < 0.01$). *D,* in resting MSNs, spontaneous mitochondrial superoxide flashes occurred at a significantly higher frequency in YAC128 neurons than in WT neurons (**, $p < 0.01$). In response to DHPG, superoxide flashes in both WT ($n = 11$) and YAC128 MSNs ($n = 7$) occurred at a significantly higher frequency when compared with resting MSNs (**, $p < 0.01$), and DHPG induced a significantly higher flash frequency in YAC128 MSNs ($n = 7$) compared with that in WT MSNs ($n = 11$) (*, $p < 0.05$). Flashes occurring 5 min before and 5 min after DHPG application were averaged for superoxide flash frequency analysis. Similar results were obtained in three independent experiments. Data are shown as the mean ± S.E.

culated the number of flashes occurring per neuron in 1 min to indicate the flash frequency. A striking difference in flash frequency between WT and YAC128 MSNs was already seen in resting cells ($p < 0.01$) (Fig. 6*D*). Stimulation with DHPG significantly increased the frequencies of superoxide flashes both in WT MSNs ($p < 0.01$) and YAC128 MSNs ($p < 0.01$) (Fig. 6*D*). Furthermore, DHPG induced significantly higher flash frequencies in YAC128 MSNs compared with WT MSNs ($p < 0.01$) (Fig. 6*D*). Therefore, the amplitudes and frequencies of both spontaneous and DHPG-stimulated superoxide flashes are significantly higher in YAC128 MSNs compared with WT MSNs, indicating that mitochondria in HD striatal neuronal cells produce elevated levels of oxidative stress.

Disrupted Mitochondrial Ca^{2+} Signaling and Excessive ROS Generation in HD Patient Fibroblasts—Mitochondrial Ca^{2+} signaling dynamics and superoxide flashes were also visualized in human fibroblasts from healthy individuals and HD patients. Similar to YAC128 MSNs, HD patient fibroblasts also showed a significantly higher level of mitochondrial Ca^{2+} loading compared with healthy fibroblasts (Fig. 7, *A–C*), indicating that mitochondrial Ca^{2+} signaling is also disrupted in HD patient fibroblasts. Furthermore, the amplitudes and frequencies of both spontaneous and BK-stimulated superoxide flashes were significantly higher in HD patient fibroblasts compared with

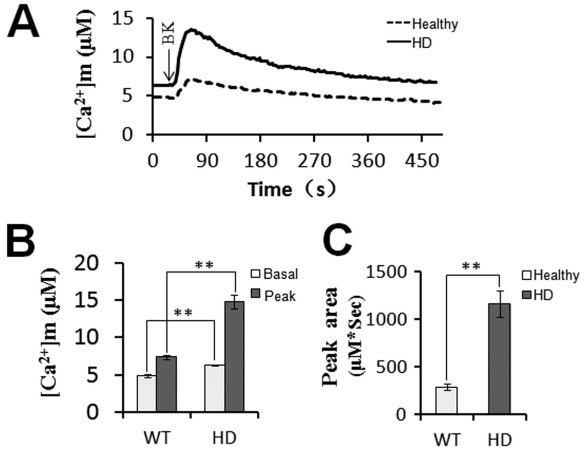

FIGURE 7. **Disrupted mitochondrial Ca^{2+} signaling in HD patient fibroblasts.** *A,* healthy and HD patient fibroblasts were used for mitochondrial cameleon imaging experiments. Fret/donor ratio recordings were converted to absolute $[Ca^{2+}]_m$. Mitochondrial Ca^{2+} concentration traces in response to 2.5 μM BK in healthy ($n = 10$) and HD patient fibroblasts ($n = 12$) are shown. $[Ca^{2+}]_m$ traces in *A* are shown as an average of all cells in one experiment. Similar results were obtained in three independent experiments. *B* and *C,* significantly larger $[Ca^{2+}]_m$ transients were found in HD patient fibroblasts. Both basal and peak values (*B*) and peak area (*C*) were significantly higher in HD patient fibroblast mitochondria than in healthy fibroblast mitochondria in response to BK (**, $p < 0.01$). Data are shown as the mean ± S.E.

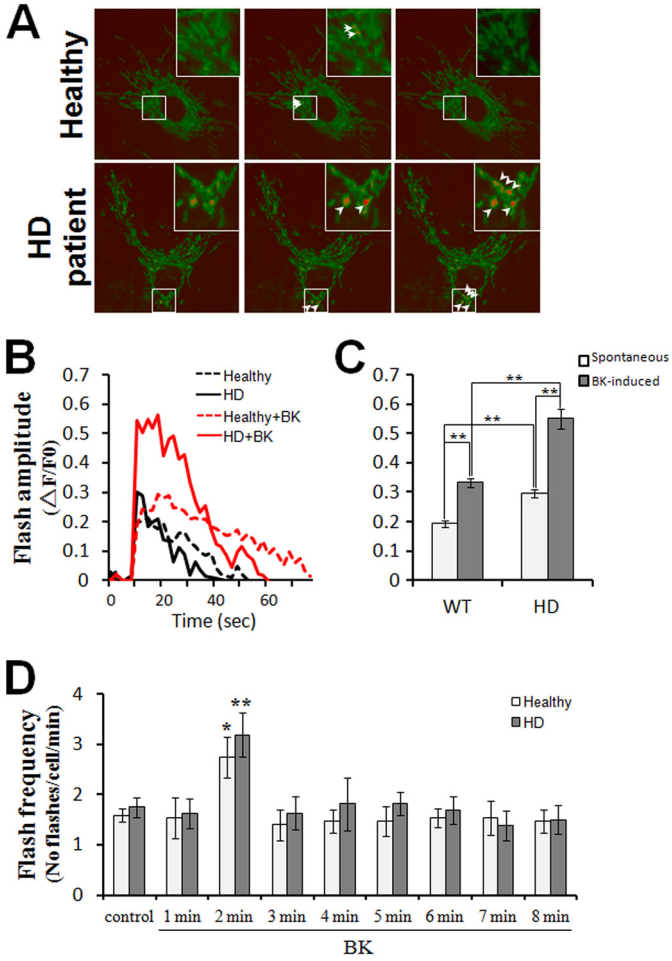

FIGURE 8. **BK promotes superoxide flash generation in HD patient fibroblasts.** *A,* representative mt-cpYFP images showing superoxide flashes in mitochondria of healthy and HD patient fibroblasts. *Arrowheads* depict individual mitochondria with superoxide flashes. *Insets* are enlarged views showing mitochondria undergoing superoxide flashes. *B,* representative mitochondrial superoxide flash traces (mt-cpYFP fluorescence with excitation at 488 nm, $\Delta F/F_0$) in healthy and HD patient fibroblasts without or with 2.5 μM BK stimulation. *C* and *D,* statistical analysis of superoxide flashes in healthy and HD patient fibroblasts in response to 2.5 μM BK. *C,* in resting cells, the amplitude of spontaneous mitochondrial superoxide flashes in HD patient fibroblasts ($n = 18$) was significantly higher than that in healthy fibroblasts ($n = 17$) (**, $p < 0.01$). In response to BK, both healthy ($n = 15$) and HD patient fibroblasts ($n = 16$) showed significantly higher amplitudes of superoxide flashes when compared with spontaneous flashes in resting MEFs (**, $p < 0.01$), and BK caused significantly higher amplitudes of superoxide flashes in HD patient fibroblasts ($n = 16$) than in healthy ($n = 15$) fibroblasts (**, $p < 0.01$). *D,* in resting cells, spontaneous mitochondrial superoxide flashes occurred at a similar frequency in healthy and HD patient fibroblasts ($p > 0.05$). In response to BK, superoxide flashes in both healthy and HD patient fibroblasts occurred at a significantly higher frequency at 2 min after BK treatment when compared with resting cells (*, $p < 0.05$; **, $p < 0.01$). Data are shown as the mean ± S.E.

healthy fibroblasts (Fig. 8, *A–D*), demonstrating that mitochondria in HD patient fibroblasts produce elevated oxidative stress.

Mitochondrial Ca^{2+} Loading Induces Elevated Mitochondrial Genomic DNA Damage in HD Cells—Age-dependent increases in mitochondrial DNA damage have been reported in the 3-nitropropionic acid-induced HD model and in R6/2 HD mice (64), although the underlying mechanism is not clear. Based on our results described above, excessive mitochondrial Ca^{2+} loading-dependent ROS generation might be responsible. We employed a quantitative PCR technique to check whether mitochondrial Ca^{2+} loading causes oxidative damage to mtDNA. The qPCR assay is based on the principle that DNA lesion blocks the progression of the DNA polymerase during PCR, resulting in decreased amplification of the fragment of interest. Thus, the amount of PCR amplification is inversely proportional to the extent of DNA damage on a given template. BK-stimulated WT and YAC128 MEFs show significant decreases in relative amplification, 50 and 69%, respectively, compared with control groups (Fig. 9, *A* and *C*), indicating damage to mtDNA. Pretreatment with MCU blocker, Ru360, or the mitochondrion-targeted antioxidant peptide, SS31, almost completely prevented the BK-induced decrease in relative amplifications (Fig. 9, *A* and *C*). The frequency of mtDNA lesions in BK-stimulated MEFs was 0.70 lesions/10 kb for WT and 1.29 lesions/10 kb for YAC128, indicating that BK induces an almost 2-fold higher level of mtDNA damage in YAC128 HD MEFs compared with WT MEFs during matrix Ca^{2+} loading (Fig. 9*D*). Ru360 can significantly reduce the BK-stimulated mtDNA damage to 0.18 lesions/10 kb for WT and 0.29 lesions/10 kb for YAC128, and SS31 significantly reduces the BK-stimulated mtDNA damage to 0.18 lesions/10 kb for WT and 0.37 lesions/10 kb for YAC128, demonstrating that the BK-stimulated increase in mtDNA damage is mitochondrial matrix Ca^{2+} loading-dependent and matrix oxidant-dependent (Fig. 9*D*). Our mtDNA damage assay data clearly revealed that disturbed mitochondrial Ca^{2+} signaling in HD cells causes excessive oxidant generation, which in turn leads to more serious mtDNA oxidative damage in HD cells. It should be noted that this repetitive BK-stimulated increase in mtDNA lesions may occur transiently, and most of the mtDNA damage could be repaired by the base excision repair pathway (65, 66). However, a significantly higher level of mtDNA damage in HD cell is expected to accumulate mtDNA lesions much faster than WT cells.

DISCUSSION

The mechanisms causing elevated oxidative stress in HD neurons remain elusive. By using a highly sensitive mitochondrial matrix-targeted superoxide indicator, cpYFP, which can sense bursts of superoxide generation *in situ* in living cells (40), we show that, even in resting cells, mitochondria in HD cells exhibit strikingly higher mitochondrial Ca^{2+} loading and oxidant generation, which in turn causes a significantly higher rate of mtDNA damage accumulation in HD cells. Steady buildup of oxidative damage to mitochondrial DNA could eventually result in mitochondrial dysfunction and be central to the etiology of HD.

Mitochondria are not only central to energy metabolism but are also a very efficient Ca^{2+} buffer system. Mitochondria are spatially and functionally organized in a network of dynamically interconnected organelles and are often in close contact with the ER and intracellular Ca^{2+}-releasing channels (57). Once Ca^{2+} is released from the ER into the cytoplasm, mitochondria take up a portion of the released Ca^{2+} primarily via the MCU at the expense of mitochondrial membrane potential ($\Delta\Psi_m$) (67). Recently, a number of studies have indicated that toxicity of HTT^{exp} may involve disturbed glutamate-induced Ca^{2+} signaling in HD medium spiny neurons (15–22, 68). $InsP_3R1$ is an

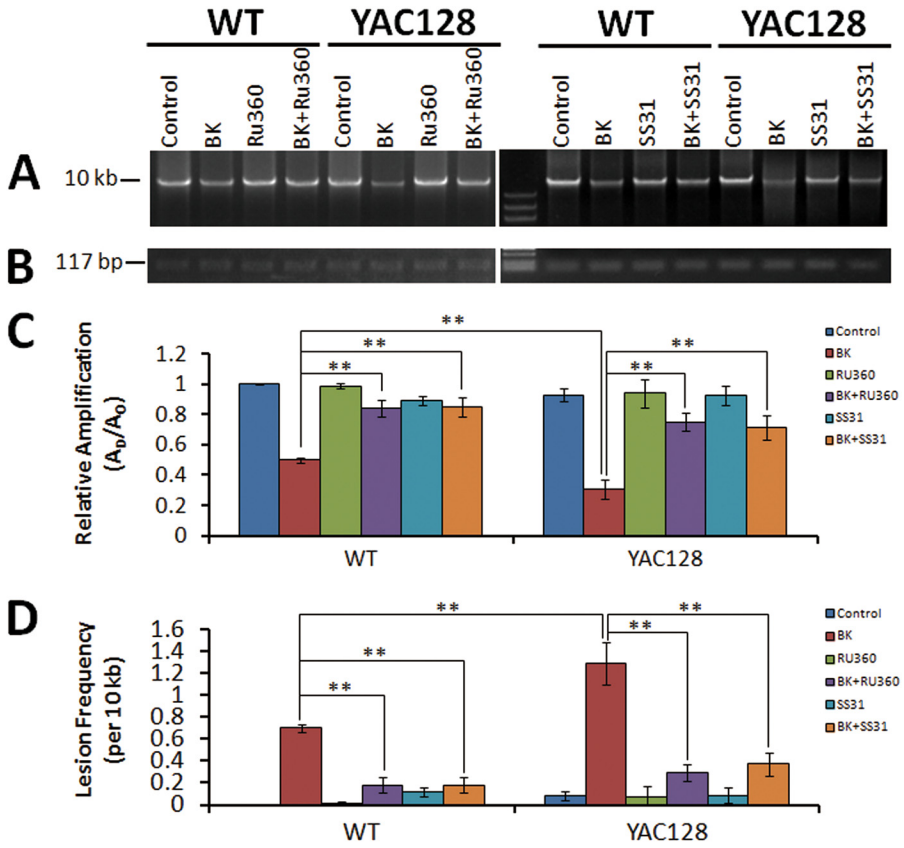

FIGURE 9. **Mitochondrial Ca^{2+} loading induces elevated mitochondrial DNA damage in YAC128 MEFs.** Total DNA samples extracted from WT and YAC128 MEFS before and after repetitive BK stimulation (twice for 10 min) without or with Ru360 and SS31 pretreatment were used for real time PCR analysis. *A,* representative agarose gel showing the amplification of a 10-kb mtDNA fragment from WT and YAC128 MEFs before and after BK stimulation. *B,* representative agarose gel showing the amplification of a 117-bp mtDNA fragment. *C,* statistical analysis of the relative levels of amplification of the mtDNA fragments before and after BK stimulation without or with Ru360 and SS31 pretreatment. Amplification of the 10-kb mtDNA fragment was normalized to the amplification of the 117-bp mtDNA fragment. Because the DNA polymerase amplifies only undamaged templates, relative amplification (A_D/A_O) is inversely proportional to the presence of damage. A_D = amount of amplification from damaged DNA sample; A_O = amount of amplification from undamaged DNA sample. *D,* comparison of mtDNA lesion frequencies from WT and YAC128 MEFs. The mean lesion frequency per 10 kb per strand was calculated using the Poisson equation as described under "Experimental Procedures." In response to the twice for 10 min BK treatment, both WT ($n = 6$) and YAC128 MEFs ($n = 6$) showed significantly higher mtDNA lesion frequencies compared with control MEFs ($p < 0.01$), and BK caused significantly higher mtDNA lesion frequencies in YAC128 MEFs than in WT MEFs (**, $p < 0.01$). Pretreatment with MCU blocker, Ru360, and mitochondrion-targeted antioxidant peptide, SS31, significantly reduced BK-induced elevation of mtDNA lesion frequencies in both WT and YAC128 MEFs (**, $p < 0.01$). Similar results were obtained in three independent experiments. Data are shown as mean ± S.E.

intracellular Ca^{2+}-releasing channel located on the ER, and HTT^{exp} binds directly and specifically to the $InsP_3R1$ C-terminal region and facilitates the sensitivity of $InsP_3R1$ to activation by $InsP_3$ (22). It is conceivable that mitochondrial Ca^{2+} loading is excessive in HD striatal neurons due to the potentiation of Ca^{2+} releasing activity of $InsP_3R1$. Indeed, we found that the amount of mitochondrial Ca^{2+} loading in HD cells was 2–4-fold higher than in WT MEFs (Fig. 1) or WT MSNs (Fig. 5) during intracellular Ca^{2+} mobilization. Our evidence also demonstrated that Ca^{2+} release via $InsP_3R1$ (Fig. 2) and the mitochondrial Ca^{2+} uniporter (Fig. 2) are all important for excessive Ca^{2+} loading into mitochondria. Our data indicate that disturbed cytosolic Ca^{2+} mobilization can directly cause disrupted mitochondrial Ca^{2+} signaling in HD neurons.

Altered mitochondrial Ca^{2+} handling in HD cells has been previously implicated in HTT^{exp} toxicity (69). Mitochondria isolated from HD patient lymphoblasts and from transgenic HD mouse brain have a lower membrane potential and are more sensitive to Ca^{2+}-mediated mPTP opening (70), and mitochondria in MSNs from HD mice have enhanced loss of $\Delta\Psi_m$ and enhanced mPTP opening in response to acute glutamate or NMDA stimulation compared with wild-type control mice (23, 51, 71). In this study, by monitoring mitochondrial matrix Ca^{2+} dynamics *in situ* and in real time, we provide direct evidence of a strikingly higher level of mitochondrial Ca^{2+} uptake during Ca^{2+} mobilization in HD neurons. Furthermore, different from our previous basal cytosolic Ca^{2+} level measurement results, we here observed significantly higher basal mitochondrial Ca^{2+} levels in HD cells (including MEFs, MSNs, and human fibroblasts) compared with those in WT/healthy cells even without stimulation. This suggested that InsP3R is more active at the resting state in HD cells than in WT cells and that this extra released Ca^{2+} was largely loaded into mitochondria and elevated the basal mitochondrial Ca^{2+} levels in HD cells. This is in agreement with a recent finding that HD cells have higher store-operated Ca^{2+} entry activity than WT cells (72), implying a constant level of ER depletion (in other words, Ca^{2+} release from ER) in HD cells. Besides the direct effect of HTT^{exp} on mitochondrial Ca^{2+} retention capacity (70), our observations of excessive mitochondrial matrix Ca^{2+} loading provide

another explanation for the mitochondrial Ca^{2+} defect observed in HD cells, and higher matrix Ca^{2+} loading could result in higher probability of mPTP open to release matrix Ca^{2+} into cytosol in HD cells.

Mitochondria constitute the major ROS generator in eukaryotic cells, including neurons. ROS are primarily produced as by-products of mitochondrial respiration due to electrons leaking from the electron transfer chain. It has long been of great interest to quantitatively monitor mitochondrial matrix ROS production *in situ* in live cells. By using the recently developed cpYFP, a highly sensitive superoxide indicator (40, 41), we quantitatively estimated mitochondrial superoxide generation *in situ* in HD MEFs and MSNs. HD cells exhibit significantly higher superoxide flash amplitudes and frequencies compared with WT cells (Figs. 3, 6, and 8), suggesting that mitochondria in HD cells are producing excessive ROS. More importantly, the elevated ROS generation in HD cells is mitochondrial matrix Ca^{2+}-dependent, because higher basal mitochondrial Ca^{2+} levels and greater mitochondrial Ca^{2+} loading in HD cells promoted ROS generation, whereas blockage of mitochondrial Ca^{2+} loading diminished the elevated superoxide flashes seen in HD cells (Figs. 3 and 4), indicating the causal link between increased mitochondrial matrix Ca^{2+} loading, elevated superoxide generation, and mtDNA damage in HD cells/neurons. Striatal neurons are most affected in HD. The striatal neurons particularly accumulate more mitochondrial genomic DNA (mtDNA) mutations than any other brain cells (27), suggesting that there is a brain regional specificity of oxidative damage in the HD patient. It has been reported that, due to the preferential expression of metabotropic glutamate receptor 1/5 (coupling to phospholipase C-inositol 1,4,5-trisphosphate pathway that can trigger $InsP_3R$ open) and NR2B NMDA receptor in striatal MSN, Htt^{exp} preferentially augments intracellular Ca^{2+} signaling in striatal MSN (18, 21, 22). Moreover, it has been reported that $InsP_3R$-mediated calcium signaling can be further enhanced by the dopamine D_1-class receptor that is primarily expressed in striatal MSN (73). Therefore, excessive mitochondrial Ca^{2+} loading and elevated mitochondrial oxidant stress are expected to occur selectively in the striatal region, which may explain why striatal neurons accumulate more mtDNA mutations than other brain cells.

Exactly how mitochondrial matrix Ca^{2+} loading stimulates ROS production remains an open question. Our results show that an increase in mitochondrial Ca^{2+} uptake was closely correlated with higher mitochondrial superoxide flash generation (Figs. 3, 4, 6, and 8). This is in agreement with recent findings that Ca^{2+} influx through L-type Ca^{2+} channels during pacemaking increases mitochondrial Ca^{2+} loading and oxidant stress in substantia nigra pars compacta dopaminergic neurons (74). One possibility is that matrix Ca^{2+} loading induces ROS production simply by stimulating the tricarboxylic acid cycle and increasing electron flux (38). Another possibility is that matrix Ca^{2+} loading induces transient openings, or flickers, of the mPTP, and a brief opening of the mPTP has been reported to stimulate ROS generation (40, 75). The frequency of brief mPTP opening is primarily determined by the matrix Ca^{2+} concentration (76). Therefore, higher matrix Ca^{2+} loading may induce a higher frequency of brief mPTP opening and higher superoxide flash generation in HD mitochondria.

As an ROS marker, superoxide flashes are bursts of superoxide generation in single mitochondria and represent the oxidative stress in mitochondria (40, 63). ROS play an important role in physiological cellular functions, such as contraction, secretion, and metabolism, but excessive ROS signals are detrimental to nucleic acids, lipids, proteins, and carbohydrates. There is a delicate balance in mitochondria between ROS generation and ROS removal to maintain a physiological oxidative homeostasis. Both overproduction of ROS and/or a deficit in the ROS defense system could disrupt this balance and cause oxidative stress. This study revealed that, due to the excess mitochondrial Ca^{2+} loading, mitochondria in HD neurons are producing significantly higher levels of ROS. Recently, Li *et al.* (77) showed that impairment of cysteine uptake led to a decline of antioxidant synthesis in HD neurons expressing full-length HTT^{exp} protein. Therefore, both overproduction of ROS and deficiency in ROS defense systems may account for the elevated oxidative stress in HD neurons.

Mitochondria are not only the major ROS producer but are also the main target of ROS. Overproduction of ROS in HD neurons causes oxidative damage to mitochondrial nucleic acids, proteins, and lipids, which in turn impair the function of mitochondria. Naked mitochondrial genomic DNA (part of which encodes subunits of complex I, III, IV, and V) and the iron-sulfur cluster-containing proteins, including the succinate dehydrogenase B subunit of complex II and the Rieske protein of complex III, are particularly vulnerable to oxidative stress (30, 78, 79). Postmortem studies of symptomatic HD patients revealed a drastic deficiency of complexes II and III and a lesser deficiency of complex IV in the caudate or putamen, with relatively normal levels in the frontal cortex or cerebellum (31, 32). Studies with HD cell models expressing *Htt* exon-1 containing elongated CAG repeats showed decreased complex II enzymatic activity and deficiency of complex III (33, 80, 81). These observations suggest that impairment of mitochondrial function is important in the progression of the disease. However, no significant deficiency of respiratory chain complexes has been demonstrated in presymptomatic patients or in HD model mice expressing full-length HTT^{exp}, suggesting that respiratory chain defects are a secondary feature in HD pathogenesis (34, 35). Based on our results showing excessive mitochondrial ROS generation and greater mtDNA damage in HD cells/neurons (Figs. 3, 4, 6, 8, and 9), it is plausible that excess Ca^{2+} loading-dependent mitochondrial oxidant stress could be a primary contributor to the respiratory chain complex defects. The appearance of mitochondrial dysfunction in advanced HD may be the result of a gradual accumulation of oxidative damage to mitochondrial proteins, DNA, and lipids due to excessive ROS production. Indeed, in this study, for the first time, we show that repetitive BK application led to increased damage of mitochondrial genomic DNA in HD cells (Fig. 9). This observation strongly supports the role of elevated ROS levels in damaging mitochondrial genomic DNA in HD. Because the mitochondrial oxidant stress in HD cells/neurons was attenuated by exposure to an $InsP_3R$ blocker, an MCU blocker (Fig. 4), and a mitochondrial antioxidant (Fig. 9), our data also suggest that a

combination of Ca^{2+} blockers and antioxidants may form a potential neuroprotective strategy for HD.

Acknowledgments—We thank Wenjuan Xie and Feilong Zhao for help with maintaining the YAC128 mouse colony and with neuronal cell culture; Ilya Bezprozvanny for facilitating transportation of mice and plasmids and for helpful discussion and critical comments on the manuscript; Roger Tsien for providing cameleon plasmids; Amy Palmer and Qi Ma for technical advice; Gang Wang for FRET technical support, and Yongliang Zhao for help with the mtDNA damage assay.

REFERENCES

1. Vonsattel, J. P., and DiFiglia, M. (1998) Huntington disease. *J. Neuropathol. Exp. Neurol.* **57,** 369–384
2. MacDonald, M. E. (2003) Huntingtin. Alive and well and working in middle management. *Science's STKE 2003,* pe48
3. The Huntington Disease Collaborative Research and Group (1993) A novel gene containing a trinucleotide repeat that is expanded and unstable on Huntington's disease chromosomes. The Huntington's Disease Collaborative Research Group. *Cell* **72,** 971–983
4. Tobin, A. J., and Signer, E. R. (2000) Huntington's disease. The challenge for cell biologists. *Trends Cell Biol.* **10,** 531–536
5. Ross, C. A. (2002) Polyglutamine pathogenesis. Emergence of unifying mechanisms for Huntington's disease and related disorders. *Neuron* **35,** 819–822
6. Harjes, P., and Wanker, E. E. (2003) The hunt for huntingtin function. Interaction partners tell many different stories. *Trends Biochem. Sci.* **28,** 425–433
7. Trushina, E., Heldebrant, M. P., Perez-Terzic, C. M., Bortolon, R., Kovtun, I. V., Badger, J. D., 2nd, Terzic, A., Estévez, A., Windebank, A. J., Dyer, R. B., Yao, J., and McMurray, C. T. (2003) Microtubule destabilization and nuclear entry are sequential steps leading to toxicity in Huntington's disease. *Proc. Natl. Acad. Sci. U.S.A.* **100,** 12171–12176
8. Sugars, K. L., and Rubinsztein, D. C. (2003) Transcriptional abnormalities in Huntington disease. *Trends Genet.* **19,** 233–238
9. Bezprozvanny, I., and Hayden, M. R. (2004) Deranged neuronal calcium signaling and Huntington disease. *Biochem. Biophys. Res. Commun.* **322,** 1310–1317
10. Cornett, J., Cao, F., Wang, C. E., Ross, C. A., Bates, G. P., Li, S. H., and Li, X. J. (2005) Polyglutamine expansion of huntingtin impairs its nuclear export. *Nat. Genet.* **37,** 198–204
11. Li, S., and Li, X. J. (2006) Multiple pathways contribute to the pathogenesis of Huntington disease. *Mol. Neurodegeneration* **1,** 19
12. Cui, L., Jeong, H., Borovecki, F., Parkhurst, C. N., Tanese, N., and Krainc, D. (2006) Transcriptional repression of PGC-1α by mutant huntingtin leads to mitochondrial dysfunction and neurodegeneration. *Cell* **127,** 59–69
13. Trushina, E., and McMurray, C. T. (2007) Oxidative stress and mitochondrial dysfunction in neurodegenerative diseases. *Neuroscience* **145,** 1233–1248
14. Fan, M. M., and Raymond, L. A. (2007) *N*-Methyl-D-aspartate (NMDA) receptor function and excitotoxicity in Huntington's disease. *Prog. Neurobiol.* **81,** 272–293
15. Heng, M. Y., Detloff, P. J., Wang, P. L., Tsien, J. Z., and Albin, R. L. (2009) *In vivo* evidence for NMDA receptor-mediated excitotoxicity in a murine genetic model of Huntington disease. *J. Neurosci.* **29,** 3200–3205
16. Bezprozvanny, I. (2009) Calcium signaling and neurodegenerative diseases. *Trends Mol. Med.* **15,** 89–100
17. Sun, Y., Savanenin, A., Reddy, P. H., and Liu, Y. F. (2001) Polyglutamine-expanded huntingtin promotes sensitization of *N*-methyl-D-aspartate receptors via post-synaptic density 95. *J. Biol. Chem.* **276,** 24713–24718
18. Zeron, M. M., Hansson, O., Chen, N., Wellington, C. L., Leavitt, B. R., Brundin, P., Hayden, M. R., and Raymond, L. A. (2002) Increased sensitivity to *N*-methyl-D-aspartate receptor-mediated excitotoxicity in a mouse model of Huntington's disease. *Neuron* **33,** 849–860
19. Song, C., Zhang, Y., Parsons, C. G., and Liu, Y. F. (2003) Expression of polyglutamine-expanded huntingtin induces tyrosine phosphorylation of *N*-methyl-D-aspartate receptors. *J. Biol. Chem.* **278,** 33364–33369
20. Shehadeh, J., Fernandes, H. B., Zeron Mullins, M. M., Graham, R. K., Leavitt, B. R., Hayden, M. R., and Raymond, L. A. (2006) Striatal neuronal apoptosis is preferentially enhanced by NMDA receptor activation in YAC transgenic mouse model of Huntington disease. *Neurobiol. Dis.* **21,** 392–403
21. Fan, M. M., Fernandes, H. B., Zhang, L. Y., Hayden, M. R., and Raymond, L. A. (2007) Altered NMDA receptor trafficking in a yeast artificial chromosome transgenic mouse model of Huntington's disease. *J. Neurosci.* **27,** 3768–3779
22. Tang, T.-S., Tu, H., Chan, E. Y., Maximov, A., Wang, Z., Wellington, C. L., Hayden, M. R., and Bezprozvanny, I. (2003) Huntingtin and huntingtin-associated protein 1 influence neuronal calcium signaling mediated by inositol-(1,4,5) triphosphate receptor type 1. *Neuron* **39,** 227–239
23. Tang, T. S., Slow, E., Lupu, V., Stavrovskaya, I. G., Sugimori, M., Llinás, R., Kristal, B. S., Hayden, M. R., and Bezprozvanny, I. (2005) Disturbed Ca^{2+} signaling and apoptosis of medium spiny neurons in Huntington's disease. *Proc. Natl. Acad. Sci. U.S.A.* **102,** 2602–2607
24. Lin, M. T., and Beal, M. F. (2006) Mitochondrial dysfunction and oxidative stress in neurodegenerative diseases. *Nature* **443,** 787–795
25. Horton, T. M., Graham, B. H., Corral-Debrinski, M., Shoffner, J. M., Kaufman, A. E., Beal, M. F., and Wallace, D. C. (1995) Marked increase in mitochondrial DNA deletion levels in the cerebral cortex of Huntington's disease patients. *Neurology* **45,** 1879–1883
26. Polidori, M. C., Mecocci, P., Browne, S. E., Senin, U., and Beal, M. F. (1999) Oxidative damage to mitochondrial DNA in Huntington's disease parietal cortex. *Neurosci. Lett.* **272,** 53–56
27. Cantuti-Castelvetri, I., Lin, M. T., Zheng, K., Keller-McGandy, C. E., Betensky, R. A., Johns, D. R., Beal, M. F., Standaert, D. G., and Simon, D. K. (2005) Somatic mitochondrial DNA mutations in single neurons and glia. *Neurobiol. Aging* **26,** 1343–1355
28. Pérez-Severiano, F., Ríos, C., and Segovia, J. (2000) Striatal oxidative damage parallels the expression of a neurological phenotype in mice transgenic for the mutation of Huntington's disease. *Brain Res.* **862,** 234–237
29. Shirendeb, U., Reddy, A. P., Manczak, M., Calkins, M. J., Mao, P., Tagle, D. A., and Reddy, P. H. (2011) Abnormal mitochondrial dynamics, mitochondrial loss and mutant huntingtin oligomers in Huntington's disease. Implications for selective neuronal damage. *Hum. Mol. Genet.* **20,** 1438–1455
30. Santos, J. H., Hunakova, L., Chen, Y., Bortner, C., and Van Houten, B. (2003) Cell sorting experiments link persistent mitochondrial DNA damage with loss of mitochondrial membrane potential and apoptotic cell death. *J. Biol. Chem.* **278,** 1728–1734
31. Gu, M., Gash, M. T., Mann, V. M., Javoy-Agid, F., Cooper, J. M., and Schapira, A. H. (1996) Mitochondrial defect in Huntington's disease caudate nucleus. *Ann. Neurol.* **39,** 385–389
32. Browne, S. E., Bowling, A. C., MacGarvey, U., Baik, M. J., Berger, S. C., Muqit, M. M., Bird, E. D., and Beal, M. F. (1997) Oxidative damage and metabolic dysfunction in Huntington's disease. Selective vulnerability of the basal ganglia. *Ann. Neurol.* **41,** 646–653
33. Benchoua, A., Trioulier, Y., Zala, D., Gaillard, M. C., Lefort, N., Dufour, N., Saudou, F., Elalouf, J. M., Hirsch, E., Hantraye, P., Déglon, N., and Brouillet, E. (2006) Involvement of mitochondrial complex II defects in neuronal death produced by N-terminal fragment of mutated huntingtin. *Mol. Biol. Cell* **17,** 1652–1663
34. Guidetti, P., Charles, V., Chen, E. Y., Reddy, P. H., Kordower, J. H., Whetsell, W. O., Jr., Schwarcz, R., and Tagle, D. A. (2001) Early degenerative changes in transgenic mice expressing mutant huntingtin involve dendritic abnormalities but no impairment of mitochondrial energy production. *Exp. Neurol.* **169,** 340–350
35. Browne, S. E. (2008) Mitochondria and Huntington's disease pathogenesis. Insight from genetic and chemical models. *Ann. N.Y. Acad. Sci.* **1147,** 358–382
36. Brand, M. D., and Esteves, T. C. (2005) Physiological functions of the mitochondrial uncoupling proteins UCP2 and UCP3. *Cell Metab.* **2,**

85–93
37. Viola, H. M., Arthur, P. G., and Hool, L. C. (2007) Transient exposure to hydrogen peroxide causes an increase in mitochondria-derived superoxide as a result of sustained alteration in L-type Ca^{2+} channel function in the absence of apoptosis in ventricular myocytes. *Circ. Res.* **100,** 1036–1044
38. Brookes, P. S., Yoon, Y., Robotham, J. L., Anders, M. W., and Sheu, S. S. (2004) Calcium, ATP, and ROS: a mitochondrial love-hate triangle. *Am. J. Physiol. Cell Physiol.* **287,** C817–C833
39. Feissner, R. F., Skalska, J., Gaum, W. E., and Sheu, S. S. (2009) Cross-talk signaling between mitochondrial Ca^{2+} and ROS. *Front. Biosci.* **14,** 1197–1218
40. Wang, W., Fang, H., Groom, L., Cheng, A., Zhang, W., Liu, J., Wang, X., Li, K., Han, P., Zheng, M., Yin, J., Wang, W., Mattson, M. P., Kao, J. P., Lakatta, E. G., Sheu, S. S., Ouyang, K., Chen, J., Dirksen, R. T., and Cheng, H. (2008) Superoxide flashes in single mitochondria. *Cell* **134,** 279–290
41. Fang, H., Chen, M., Ding, Y., Shang, W., Xu, J., Zhang, X., Zhang, W., Li, K., Xiao, Y., Gao, F., Shang, S., Li, J. C., Tian, X. L., Wang, S. Q., Zhou, J., Weisleder, N., Ma, J., Ouyang, K., Chen, J., Wang, X., Zheng, M., Wang, W., Zhang, X., and Cheng, H. (2011) Imaging superoxide flash and metabolism-coupled mitochondrial permeability transition in living animals. *Cell Res.* **21,** 1295–1304
42. Palmer, A. E., Giacomello, M., Kortemme, T., Hires, S. A., Lev-Ram, V., Baker, D., and Tsien, R. Y. (2006) Ca^{2+} indicators based on computationally redesigned calmodulin-peptide pairs. *Chem. Biol.* **13,** 521–530
43. McCombs, J. E., and Palmer, A. E. (2008) Measuring calcium dynamics in living cells with genetically encodable calcium indicators. *Methods* **46,** 152–159
44. Bano, D., Young, K. W., Guerin, C. J., Lefeuvre, R., Rothwell, N. J., Naldini, L., Rizzuto, R., Carafoli, E., and Nicotera, P. (2005) Cleavage of the plasma membrane Na^+/Ca^{2+} exchanger in excitotoxicity. *Cell* **120,** 275–285
45. Choe, C. U., and Ehrlich, B. E. (2006) The inositol 1,4,5-trisphosphate receptor (IP3R) and its regulators. Sometimes good and sometimes bad teamwork. *Science's STKE 2006,* re15
46. Chan, C. S., Guzman, J. N., Ilijic, E., Mercer, J. N., Rick, C., Tkatch, T., Meredith, G. E., and Surmeier, D. J. (2007) "Rejuvenation" protects neurons in mouse models of Parkinson's disease. *Nature* **447,** 1081–1086
47. Surmeier, D. J. (2007) Calcium, ageing, and neuronal vulnerability in Parkinson's disease. *Lancet Neurol.* **6,** 933–938
48. Stutzmann, G. E., and Mattson, M. P. (2011) Endoplasmic reticulum Ca^{2+} handling in excitable cells in health and disease. *Pharmacol. Rev.* **63,** 700–727
49. Slow, E. J., van Raamsdonk, J., Rogers, D., Coleman, S. H., Graham, R. K., Deng, Y., Oh, R., Bissada, N., Hossain, S. M., Yang, Y. Z., Li, X. J., Simpson, E. M., Gutekunst, C. A., Leavitt, B. R., and Hayden, M. R. (2003) Selective striatal neuronal loss in a YAC128 mouse model of Huntington disease. *Hum. Mol. Genet.* **12,** 1555–1567
50. Guo, C., Tang, T. S., Bienko, M., Dikic, I., and Friedberg, E. C. (2008) Requirements for the interaction of mouse Polκ with ubiquitin and its biological significance. *J. Biol. Chem.* **283,** 4658–4664
51. Zhang, H., Li, Q., Graham, R. K., Slow, E., Hayden, M. R., and Bezprozvanny, I. (2008) Full-length mutant huntingtin is required for altered Ca^{2+} signaling and apoptosis of striatal neurons in the YAC mouse model of Huntington's disease. *Neurobiol. Dis.* **31,** 80–88
52. Isakson, B. E. (2008) Localized expression of an $Ins(1,4,5)P_3$ receptor at the myoendothelial junction selectively regulates heterocellular Ca^{2+} communication. *J. Cell Sci.* **121,** 3664–3673
53. Jones, L., Ma, L., Castro, J., Litjens, T., Barritt, G. J., and Rychkov, G. Y. (2011) The predominant role of IP_3 type 1 receptors in activation of store-operated Ca^{2+} entry in liver cells. *Biochim. Biophys. Acta* **1808,** 745–751
54. Santos, J. H., Meyer, J. N., Mandavilli, B. S., and Van Houten, B. (2006) Quantitative PCR-based measurement of nuclear and mitochondrial DNA damage and repair in mammalian cells. *Methods Mol. Biol.* **314,** 183–199
55. Ayala-Torres, S., Chen, Y., Svoboda, T., Rosenblatt, J., and Van Houten, B. (2000) Analysis of gene-specific DNA damage and repair using quantitative polymerase chain reaction. *Methods* **22,** 135–147
56. Hayashi, T., Rizzuto, R., Hajnoczky, G., and Su, T. P. (2009) MAM. More than just a housekeeper. *Trends Cell Biol.* **19,** 81–88
57. Csordás, G., Várnai, P., Golenár, T., Roy, S., Purkins, G., Schneider, T. G., Balla, T., and Hajnóczky, G. (2010) Imaging interorganelle contacts and local calcium dynamics at the ER-mitochondrial interface. *Mol. Cell* **39,** 121–132
58. Maruyama, T., Kanaji, T., Nakade, S., Kanno, T., and Mikoshiba, K. (1997) 2APB, 2-aminoethoxydiphenyl borate, a membrane-penetrable modulator of $Ins(1,4,5)P_3$-induced Ca^{2+} release. *J. Biochem.* **122,** 498–505
59. Bootman, M. D., Collins, T. J., Mackenzie, L., Roderick, H. L., Berridge, M. J., and Peppiatt, C. M. (2002) 2-Aminoethoxydiphenyl borate (2-APB) is a reliable blocker of store-operated Ca^{2+} entry but an inconsistent inhibitor of $InsP_3$-induced Ca^{2+} release. *FASEB J.* **16,** 1145–1150
60. Kirichok, Y., Krapivinsky, G., and Clapham, D. E. (2004) The mitochondrial calcium uniporter is a highly selective ion channel. *Nature* **427,** 360–364
61. Ying, W. L., Emerson, J., Clarke, M. J., and Sanadi, D. R. (1991) Inhibition of mitochondrial calcium ion transport by an oxo-bridged dinuclear ruthenium ammine complex. *Biochemistry* **30,** 4949–4952
62. McCormack, J. G., Halestrap, A. P., and Denton, R. M. (1990) Role of calcium ions in regulation of mammalian intramitochondrial metabolism. *Physiol. Rev.* **70,** 391–425
63. Ma, Q., Fang, H., Shang, W., Liu, L., Xu, Z., Ye, T., Wang, X., Zheng, M., Chen, Q., and Cheng, H. (2011) Superoxide flashes. Early mitochondrial signals for oxidative stress-induced apoptosis. *J. Biol. Chem.* **286,** 27573–27581
64. Acevedo-Torres, K., Berríos, L., Rosario, N., Dufault, V., Skatchkov, S., Eaton, M. J., Torres-Ramos, C. A., and Ayala-Torres, S. (2009) Mitochondrial DNA damage is a hallmark of chemically induced and the R6/2 transgenic model of Huntington's disease. *DNA Repair* **8,** 126–136
65. Friedberg, E. C. (2003) DNA damage and repair. *Nature* **421,** 436–440
66. Mitra, S., Izumi, T., Boldogh, I., Bhakat, K. K., Chattopadhyay, R., and Szczesny, B. (2007) Intracellular trafficking and regulation of mammalian AP-endonuclease 1 (APE1), an essential DNA repair protein. *DNA Repair* **6,** 461–469
67. Tinel, H., Cancela, J. M., Mogami, H., Gerasimenko, J. V., Gerasimenko, O. V., Tepikin, A. V., and Petersen, O. H. (1999) Active mitochondria surrounding the pancreatic acinar granule region prevent spreading of inositol trisphosphate-evoked local cytosolic Ca^{2+} signals. *EMBO J.* **18,** 4999–5008
68. Lim, D., Fedrizzi, L., Tartari, M., Zuccato, C., Cattaneo, E., Brini, M., and Carafoli, E. (2008) Calcium homeostasis and mitochondrial dysfunction in striatal neurons of Huntington disease. *J. Biol. Chem.* **283,** 5780–5789
69. Choo, Y. S., Johnson, G. V., MacDonald, M., Detloff, P. J., and Lesort, M. (2004) Mutant huntingtin directly increases susceptibility of mitochondria to the calcium-induced permeability transition and cytochrome *c* release. *Hum. Mol. Genet.* **13,** 1407–1420
70. Panov, A. V., Gutekunst, C. A., Leavitt, B. R., Hayden, M. R., Burke, J. R., Strittmatter, W. J., and Greenamyre, J. T. (2002) Early mitochondrial calcium defects in Huntington's disease are a direct effect of polyglutamines. *Nat. Neurosci.* **5,** 731–736
71. Fernandes, H. B., Baimbridge, K. G., Church, J., Hayden, M. R., and Raymond, L. A. (2007) Mitochondrial sensitivity and altered calcium handling underlie enhanced NMDA-induced apoptosis in YAC128 model of Huntington's disease. *J. Neurosci.* **27,** 13614–13623
72. Wu, J., Shih, H. P., Vigont, V., Hrdlicka, L., Diggins, L., Singh, C., Mahoney, M., Chesworth, R., Shapiro, G., Zimina, O., Chen, X., Wu, Q., Glushankova, L., Ahlijanian, M., Koenig, G., Mozhayeva, G. N., Kaznacheyeva, E., and Bezprozvanny, I. (2011) Neuronal store-operated calcium entry pathway as a novel therapeutic target for Huntington's disease treatment. *Chem. Biol.* **18,** 777–793
73. Tang, T. S., Chen, X., Liu, J., and Bezprozvanny, I. (2007) Dopaminergic signaling and striatal neurodegeneration in Huntington's disease. *J. Neurosci.* **27,** 7899–7910
74. Guzman, J. N., Sanchez-Padilla, J., Wokosin, D., Kondapalli, J., Ilijic, E., Schumacker, P. T., and Surmeier, D. J. (2010) Oxidant stress evoked by pacemaking in dopaminergic neurons is attenuated by DJ-1. *Nature* **468,** 696–700
75. Hüser, J., Rechenmacher, C. E., and Blatter, L. A. (1998) Imaging the per-

meability pore transition in single mitochondria. *Biophys. J.* **74,** 2129–2137
76. Al-Nasser, I., and Crompton, M. (1986) The reversible Ca^{2+}-induced permeabilization of rat liver mitochondria. *Biochem. J.* **239,** 19–29
77. Li, X., Valencia, A., Sapp, E., Masso, N., Alexander, J., Reeves, P., Kegel, K. B., Aronin, N., and Difiglia, M. (2010) Aberrant Rab11-dependent trafficking of the neuronal glutamate transporter EAAC1 causes oxidative stress and cell death in Huntington disease. *J. Neurosci.* **30,** 4552–4561
78. Yakes, F. M., and Van Houten, B. (1997) Mitochondrial DNA damage is more extensive and persists longer than nuclear DNA damage in human cells following oxidative stress. *Proc. Natl. Acad. Sci. U.S.A.* **94,** 514–519
79. Li, Y., Huang, T. T., Carlson, E. J., Melov, S., Ursell, P. C., Olson, J. L., Noble, L. J., Yoshimura, M. P., Berger, C., Chan, P. H., Wallace, D. C., and Epstein, C. J. (1995) Dilated cardiomyopathy and neonatal lethality in mutant mice lacking manganese superoxide dismutase. *Nat. Genet.* **11,** 376–381
80. Solans, A., Zambrano, A., Rodríguez, M., and Barrientos, A. (2006) Cytotoxicity of a mutant huntingtin fragment in yeast involves early alterations in mitochondrial OXPHOS complexes II and III. *Hum. Mol. Genet.* **15,** 3063–3081
81. Fukui, H., and Moraes, C. T. (2007) Extended polyglutamine repeats trigger a feedback loop involving the mitochondrial complex III, the proteasome and huntingtin aggregates. *Hum. Mol. Genet.* **16,** 783–797